Marine and Petroleum Geology 154 (2023) 106333

Contents lists available at ScienceDirect

Marine and Petroleum Geology

journal homepage: www.elsevier.com/locate/marpetgeo

# Miocene tropical storms: Carbonate framework approaches and geochemistry proxies in a reservoir model

Orangel Aguilera [a,*], Olga M. Oliveira De Araújo [b], Ricardo Tadeu Lopes [b], Marcelo Cohen [c], Dayana Alvarado Sierra [c], Beatriz Teixeira Guimarães [c], Ana Paula Linhares [d], Félix Rodriguez [e], Manuel Moreira [f], Rut Díaz [f], Hamilton Santos Gama Filho [g], Marcelino Jose Dos Anjos [g], Daniel Lima [h], Julianny dos Santos Silva [a], Marie Joelle Giraud-López [i], Vinicius Tavares Kütter [c]

[a] Fluminense Federal University, Paleoecology and Global Changes Laboratory, Rua Marcos Waldemar de Freitas Reis, S/nº, Campus Gragoatá, Bloco M, Lab. 110, CEP 24210-201, Niterói, Rio de Janeiro, Brazil
[b] Federal University of Rio de Janeiro, Nuclear Instrumentation Laboratory, Nuclear Engineering Program/COPPE, Av. Horácio Macedo, Cidade Universitária, CEP, 21941-450, Rio de Janeiro, Brazil
[c] Federal University of Pará, Geoscience Institute, CEP, 66075-110, Belém, Pará, Brazil
[d] Museu Paraense Emilio Goeldi, Earth Sciences and Ecology Coordination, CEP 66077-830, Belém, Pará, Brazil
[e] Smithsonian Tropical Research Institute, Box 0843-03092, Balboa, Panama
[f] Fluminense Federal University, Institute of Chemistry, Environmental Geochemistry Program, CEP 24020-150, Niterói, Rio de Janeiro, Brazil
[g] Rio de Janeiro State University, Institute of Physics Armando Dias Tavares, Department of Applied Physics and Thermodynamics, CEP 20550-013, Rio de Janeiro, Brazil
[h] Museu de Paleontologia Plácido Cidade Nuvens, Universidade Regional do Cariri, CEP 63190-000, Santana Do Cariri, Ceará, Brazil
[i] Universidad Pedagógica y Tecnológica de Colómbia, Sagamoso, Calle, 4A Sur, No. 15-134, Boyacá, Colombia

ARTICLE INFO

*Keywords:*
Brazilian equatorial platform
Pirabas Formation
Heterozoan
Carbonate
Climate changes
Porosity

ABSTRACT

The Bragantina Platform is an important sedimentary package that occurs in northwestern Brazil, typically around the equatorial western Atlantic coast. Most of the latest Neogene succession of this carbonate-siliciclastic platform consists of the Pirabas Formation of Miocene age (Burdigalian to Serravalian). High-energy coastal storms and hurricanes as a consequence of trade wind anomalies during the Neogene impacted the shallow-water inner marine heterozoan assemblage deposits of the Pirabas Formation. A chaotic overlap of benthic infauna and epifauna, and of demersal and pelagic species in the same section was analyzed using petrography, petrophysics, micro- and macropaleontology, taphonomy, and geochemistry in order to understand sedimentary and paleo-environmental processes. The equatorial carbonate platform of Brazil reveals high-energy and multiple Miocene tropical storms. This high-energy wave environment caused severe damage to shallow-water heterozoan assemblages at the seafloor, resulting in chaotic faunal arrangements, and removing fine-grained particles thus improving the petrographic properties of the rock (porosity and permeability).

## 1. Introduction

The Brazilian equatorial platform is currently located along the Intertropical Convergence Zone (ITCZ). The ITCZ is characterized by a low-pressure belt that migrates with the thermal equator, resulting in a band where trade winds are responsible for heavy precipitation. However, most paleoclimatic research, including in northern Brazil, focuses on Quaternary data (Utida et al., 2019), since the last bioclast-dominated Neogene outcrops are still represented by the onshore portions of the Pirabas Formation at the marginal equatorial of the Bragantina Platform in Brazil (Rossetti, 2001; Rossetti et al., 2013; Aguilera et al., 2022).

* Corresponding author.
*E-mail addresses:* orangelaguilera@id.uff.br (O. Aguilera), olgaufrjlin@gmail.com (O.M.O. De Araújo), ricardo@lin.ufrj.br (R.T. Lopes), mcohen80@hotmail.com (M. Cohen), dayana18.alvarado@gmail.com (D.A. Sierra), beatriz.97.guimaraes@gmail.com (B.T. Guimarães), alinhares@museu-goeldi.br (A.P. Linhares), rodriguezf@si.edu (F. Rodriguez), manuel.a.moreira.r@gmail.com (M. Moreira), rutdiaz@id.uff.br (R. Díaz), hamiltongamafilho@hotmail.com (H.S. Gama Filho), marcelin@uerj.br (M.J. Dos Anjos), daniel.jmlima@urca.br (D. Lima), juliannysantos@id.uff.br (J. dos Santos Silva), mariejoellegiraudlopez@gmail.com (M.J. Giraud-López), viniciuskutter@id.uff.br (V.T. Kütter).

https://doi.org/10.1016/j.marpetgeo.2023.106333
Received 3 March 2023; Received in revised form 10 May 2023; Accepted 19 May 2023
Available online 24 May 2023

Analysis of current Brazilian wave climate (Cotrim et al., 2022) has shown that the long-term trends of the total significant wave height and wave energy flux in the South Atlantic Ocean are mostly due to swell events and the wave propagation effect from Southern Ocean storms. Severe damage to shallow water reefs in the Caribbean (5–20 m depth) was produced by high-energy wave hurricanes (Bries et al., 2004).

Coastal marine waves from high-category tropical storms in the central-western Atlantic Ocean in response to climate change during the Oligocene–Miocene transition, could result in significant oceanic anomalies on shallow-water marine platforms, affecting the littoral geomorphology and paleodiversity, especially the fossil heterozoan assemblages on the gentle slope of the Brazilian equatorial carbonate platform (Aguilera et al., 2020a, 2020b, 2022). The Oligocene–Miocene sea-level oscillations testified as a major hiatus of the sedimentary sequences (Haq et al., 1987; Kominz et al., 2008), the Mi-1 glacial event (Zachos et al., 2001; Stewart et al., 2017), and the increase in river runoff in ITCZ by precipitation in coastal areas during the middle Miocene Climatic Optimum (Herold et al., 2012).

From the Brazilian equatorial platform basins, the Oligocene–Miocene biostratigraphy records and paleoenvironmental interpretations (Abreu et al., 1986; Cruz et al., 2019) support changes in the sedimentary processes associated with paleoceanographic conditions.

Unknown paleoceanographic effects as a consequence of Neogene events in the Caribbean and northern South America triggered by tectonics (Barrera-Lopez et al., 2022) could be associated with the Oligocene–Miocene sedimentary records of high-energy coastal marine waves in tropical America, that is, the interoceanic Atlantic and Pacific seaway, and the effects along the boundary of the South American plate and the Panamanian microplate (Coates and Stallard, 2013; Montes et al., 2015; O'Dea et al., 2016; Jaramillo, 2018).

Large-scale potential Cenozoic paleoclimate models (Yan et al., 2019) have concluded that the warmer early Eocene was more favorable for storm formation over the southern hemisphere. However, as the climate cools, the genesis of storms from the southern hemisphere decreases over time.

The lack of paleoclimatic models to understand the Oligocene–Miocene ITCZ and the potential hazards of coastal high-energy storms, hurricanes, and cyclones as a consequence of trade wind anomalies can be interpreted based on the carbonate framework.

The preserved record of high-energy wave debris and the carbonate-siliciclastic bioclast framework deposits on the Brazilian equatorial platform from the late early (~16 Ma) to the late middle (13–12 Ma and younger) Miocene Pirabas Formation (Gomes et al., 2023), consists of a wide mixture of complex assemblages of heterozoan (Aguilera et al., 2020a, 2020b, 2022). Entire, disarticulated, and broken shells, bryozoan and coral fragments, and skeletal remains of fish, land reptiles, and marine mammals, arranged in a bioclastic accumulation, show an overlapping infauna and epifauna, and the overlapping of benthic, demersal, and pelagic species concentrated in the same section (Aguilera et al., 2020a, 2020b; Bencomo et al., 2021). This chaotic faunal arrangement could have resulted from heavy disturbances recorded during a storm or the superposition of multiple storm events during the time that impacted the shallow water heterozoan and bioclast framework deposits of the Pirabas Formation, particularly at the oceanfront facies from the Atlantic Ocean.

Previous discussions on the chaotic faunal arrangement of echinoderms and the infilled test by Pirabas Formation sediment were interpreted as the results of potential high-energy waves (Bencomo et al., 2021). However, reworking periods of storm waves leave diagnostic ichnological signatures in the deposits (De Araújo et al., 2021), and the fast burial sedimentary processes over mangrove floodplains from the Pirabas Formation result in well-preserved fossil crustacean infauna (Lima et al., 2020).

The geochemical fingerprints of elemental composition and mineral characterization of sedimentary rocks provide information on carbonate lithofacies and sources of terrigenous material, the climate of the surrounding landmasses, the oxygenation state of the seafloor, and oceanographic conditions (Carannante et al., 1988; Calvert and Pedersen, 2007; Govin et al., 2012; Gebregiorgis et al., 2020; De Sousa et al., 2021).

The Miocene facies model of the Pirabas Formation in the Ilha de Fortaleza at Ponta do Castelo and Fazenda outcrops was compared to those of reference samples from the outcrops and quarries of the Pirabas Formation and discussed in the context of the sedimentary and geochemical signatures.

The objective of this contribution is to identify high-energy oceanfront deposits with accurate potential tracking of local storms analysis, as pieces of evidence of high-energy multiple wave impacts.

## 2. Physical setting

The Bragantina Platform is an important sedimentary package found in the northwestern region of Brazil (Fig. 1). Most of the latest Neogene succession of this platform corresponds to the rocks of the Miocene (Burdigalian to Serravalian) of the Pirabas Formation (Gomes et al., 2023), which is characterized by carbonate-siliciclastic rocks interspersed by thin layers of greenish or dark clays, and by sandstones with calciferous cement (Rossetti et al., 2013; Aguilera et al., 2022). It is deposited over Precambrian rocks and it is overlapped with the Barreiras Formation (Rossetti et al., 1989; Rossetti, 2006).

The Brazilian equatorial margin can be categorized into three main stages: i) the pre-Amazonian stage during the Upper Cretaceous to mid-Miocene, that is, before the establishment of the transcontinental drainage of the Amazon River; ii) the Amazonian fan stage during the late Miocene to the present day, that is, after the establishment of the modern Amazon drainage system (Figueiredo et al., 2009; Gorini et al., 2014); iii) the third stage, which overlaps the late Cenozoic, is the pre-Panamanian isthmus stage and the Atlantic and the Pacific interoceanic seaway (Coates and Stallard, 2013; Montes et al., 2015; O'Dea et al., 2016; Jaramillo, 2018), delimited the equatorial margin of South America.

Based on this composition, the Pirabas Formation should have been deposited during the pre-Amazon and pre-Panamanian isthmus stages. Thus, it should record the initial stages of the progressive transition of the bioclast carbonate-dominated equatorial margin to a siliciclastic-dominated environment (Aguilera et al., 2022).

The Pirabas Formation is divided into three main facies i) the facies α1characterized by echinoderm–bryozoan packstone to rudstone rich in mollusks and soritids. These bioclastic sediments were mostly deposited in a medium to the outer inner platform; ii) the facies α2 characterized by siliciclastic-rich wackestone to packstone, represented by mixed siliciclastic and carbonate deposited from the proximal inner platform; and iii) the facies β, characterized by siliciclastic fine-grained sandstone to mudstone, locally pyrite-rich, deposited close to the coast, and dominated by terrigenous sediments (Aguilera et al., 2022). The outcrops of Ponta do Castelo and Fazenda in the Ilha de Fortaleza are included in facies α that resemble the outer inner platform exposed to oceanic influence.

## 3. Material and methods

Field trips for sample collection were conducted at two outcrops (Ponta do Castelo, 0°40′55.69″ S, 47°10′13.30″ W, and Fazenda, 0°42″43.79″ S, 47°9′58.65″W), located 3.4 km apart from the type locality of the Pirabas Formation at Ilha de Fortaleza, São João de Pirabas, Pará state, Brazil. These outcrops are mostly composed of packstone layers exposed during the low tide period and are approximately 4 m thick (Fig. 2).

High spatial resolution images of the study areas were obtained during four campaigns at the Ponta do Castelo and Fazenda outcrops (Fig. S1) using a multispectral drone. The Phantom 4 RTK images were

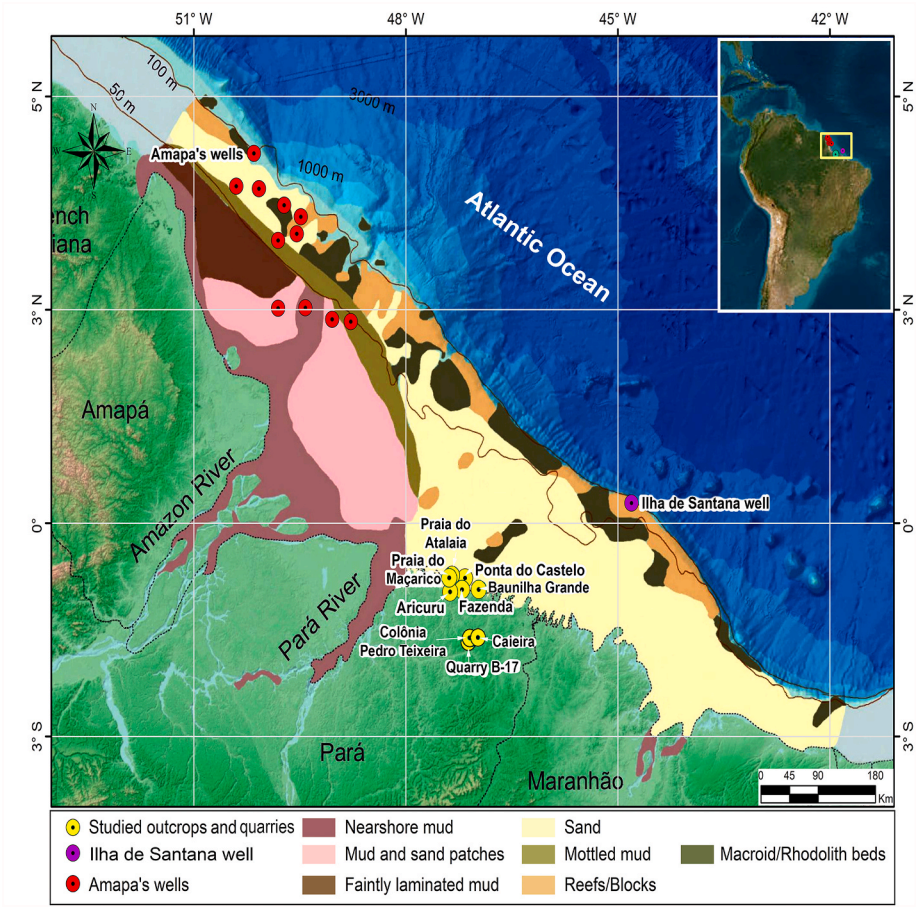


**Fig. 1.** Schematic map of the northwestern Brazilian platform modified (Banha et al., 2022; Vale et al., 2022). Light green circle: Ponta do Castelo and Fazenda outcrops studied from Ilha de Fortaleza and reference samples from other outcrops and quarry of the Pirabas Formation. Purple circle: PETROBRAS Ilha de Santana Formation well. Yellow circle: PETROBRAS Amapá Formation wells. The blue color of the nearshore water surface is removed to show the seafloor lithology (mud, sand, and rock) that is represented in specific colors following the map legend.

acquired using a FC 6310 digital 4K/20 MP (RGB). The DJI Ground Station Pro Software installed in an IPad Air tablet allowed the implementation of autonomous missions, following routes with a 90° camera angle, 90% frontal and 75% lateral overlay, at a 60 m altitude to obtain high spatial resolution (~2 cm) images. We scanned 14.3 ha (476 images) and 14.5 ha (502 images) in Fazenda and Castelo, respectively. Drone images were processed using Agisoft Metashape. Black rubber mats (1 $m^2$) marked with yellow cross-adhesive tapes were used as targets for Ground Control Points (GCP). A total of 18 GCPs were used to orthorectify the drone images. Planialtimetric data for the GCPs were obtained during fieldwork with a laser topographic leveler and a Trimble Catalyst Antenna with a Global Navigation Satellite System (GNSS). Submetric corrections were made on a Trimble basis. The planimetric and altimetric precision of the GCPs were in the order of ±30 cm. Quantitative analysis of the vertical and horizontal divergences between the checkpoints and the Digital Elevation Model was obtained using the following equation: Zdif = Z3D - Zgrd (Zdif = vertical differences, Z3D = the Z-value of the dense point cloud, Zgrd = checkpoint Z value based on GCPs) (Cohen et al., 2021). This analysis indicated Zdif values lower than 3.5 cm; then, a vertical margin of error of ±3.5 cm was admitted for the 3D models.

The samples for the macro- and micropaleontology, petrography, and microcomputer tomography analyses comprised six blocks of rocks (2 kg each), and six micro-plugs approximately of 60 mm in length and 25 mm in diameter, obtained with a portable drill. The selection criteria of samples were based on the well preserved, abundance, and diversity of fossils in the rock matrix along the section.

Macrofossil specimens were collected by hand when they were easily accessible at the sediment surface. Alternatively, when they were cemented in the rock, *in situ* digital photographs were taken, including ichnofossil galleries.

Eigth blocks of rock samples (from Ponta do Castelo and Fazenda) of approximately 1 kg each were disaggregated in hot water, sieved, and processed in the laboratory using 500 μm, 250 μm, 180 μm, and 125 μm mesh sizes. Then, the microfossil specimens were picked using a stereomicroscope, and scanning electron microscope images were obtained using a TESCAN electronic microscope Mira3, with electron gun-type field emission. The samples were mounted on aluminum supports with a diameter of 12 mm using a double-sided carbon adhesive tape. They were metalized with Au over 90 s, and the deposits on the sample created a film with an average thickness of 12 nm. The images were generated by secondary electron detection using a voltage acceleration between 5 and 1 kV in a working distance of approximately 15 mm.

For microCT acquisition, a V-Tomex-M (GE Measurement & Control Solutions, Wunstorf, Germany) was used. The 3D reconstructions were performed using Phoenix Data software, in which slice alignment, beam hardening correction, and ring artifact reduction were implemented, and a mathematical edge-enhancement filter was applied to achieve a higher contrast between the rock matrix and the pores. For the 3D visualization, VG Studio Max v 3.0 software was used.

Five sub-samples (two from the Ponta de Castelo and three from the Fazenda outcrops) were scanned for microCT acquisitions, volumetry of high-resolution macrofossil contents, and 3D individual reconstruction of specimens into the block to maintain the original plane orientation with respect to the azimuth. According to the taxa, the specimens were virtually colored to distinguish the faunal compositions. We used the mollusk shell Y axis arrangements in the real living position (Ponder et al., 2019) and the ahermatypic coral Y axis (Cairns, 2016) to estimate the azimuth on the natural plane. In addition, the echinoid test and crab carapaces were used to improve the spatial vector trend and plane changes.

To obtain quantitative information on the porosity of the sample, it

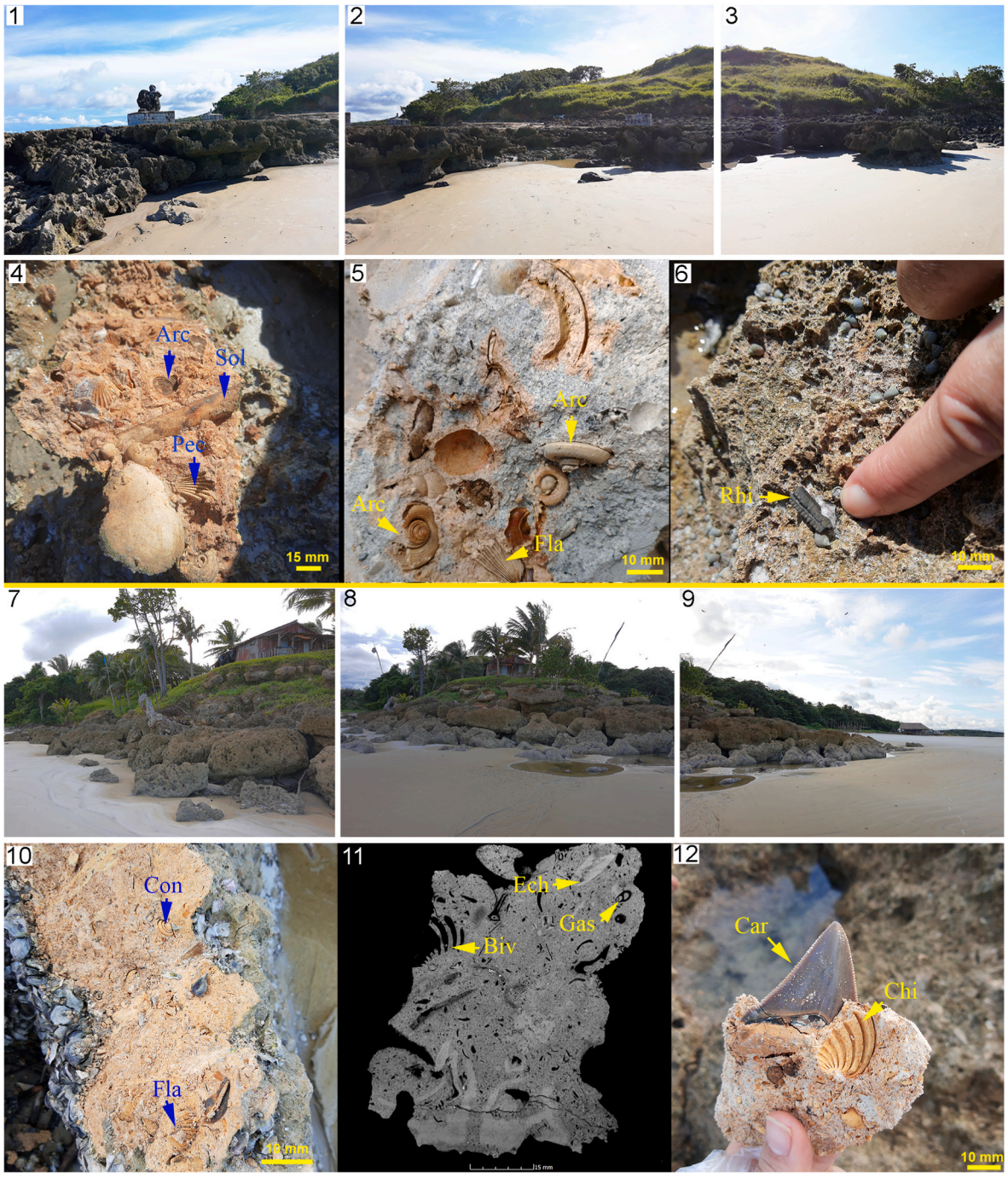


**Fig. 2.** Pirabas Formation outcrops at Ilha de Fortaleza. 1–3, landscape views of Ponta do Castelo outcrop; 4, detailed view of the exposed rock after the removal of the most superficial layer showing molds and prints of mollusks (note the horizontal arrangement of the large *Solen obliquus* (Sol) a bivalve that inhabits the soft-bottom in a vertical position, *Architectonica* sp. (Arc), and *Pecten* sp. (Pec); 5, detailed view of exposed rock showing prints and mold of *Architectonica* sp. (Arc) and *Flabellus* sp. (Fla). Note the shell dissolution produced by the diagenesis; 6, detailed view of the altered rock surface, containing an isolated tooth plate of stingray *Rhinoptera* sp. (Rhi); 7–9, landscape views of the Fazenda outcrop ; 10, detailed view of exposed rock after removing the most superficial layer showing molds and prints of the mollusk *Conus* sp. (Con), and the ahermatypic coral *Flabellus* sp. (Fla); 11, detailed micro CT image of the rock block showing echinoderm remains (Ech), gastropods (Gas), and bivalves (Biv) in a chaotic arrangement; 12, detailed view of the removed rock fragment with a tooth of the largest white shark *Carcharocles chubutensis* (Car), associated with a print of a venerid shell of *Chione* sp. (Chi).

was necessary to extract the porosity network. Segmentation was performed for this purpose. Segmentation in image processing refers to the decomposition of an object into segments, that is, the identification of discrete materials in the image. In this manner, the pores were identified and separated from the rock matrix. Following the identification and extraction of this pore network, it was possible to perform a quantitative analysis of the porosity, such as the total porosity, main channel volume, and pore diameter distribution, and estimate the permeability of the sample. Porosity analysis were performed with Avizo Fire Xlab Hydro (FEI Visual Sciences Group), solving the Stokes equations using the finite volume method.

Six thin petrographic sections of the plug subsample from the Ponta do Castelo and Fazenda outcrops were prepared for study, and the same type of analysis was performed on the Caieira (Capanema Municipality)

leaf bed blocks. The samples were fixed on 76 × 26 mm glass slides and polished to a thickness of 30 μm. Photomicrographs were obtained using a petrographic microscope equipped with an integrated digital system. We used the granulometry scale of Udden-Wentworth for the grain-size relationships.

The analysis of macrofossils taxonomy, morphology, ecology, and features, including articulation/disarticulation, infilled sediments, and encrustation, followed a general trend described by (Bencomo et al., 2021). The microfossil assemblages were studied based on individual picking samples (Aguilera et al., 2020a, 2020b) and petrographic thin sections (Aguilera et al., 2022). The taxonomy and paleoecology dataset are listed (Table S1), and follow the review of the main literature species taxonomy and the paleoecological interpretation (e.g., Foraminifera: Cann et al., 2000; Peeters et al., 2002; Javaux and Scott, 2003; Mateu-Vicens et al., 2008; Prazeres et al., 2017; Sariaslan and Langer, 2021. Ostracods: Guernet and Fourcade, 1988; Whatley and Watson, 1988; Pezelj et al., 2007; Puckett, 2008; Forsey, 2016; Bhanat et al., 2018; Şafak, 2019. Mollusk: Maury, 1925; Hendy, 2013; Hendy et al., 2015. Bryozoan: Ramalho et al., 2015, 2017, 2019; Zágoršek et al., 2014. Coral: Cairns, 2017. Echinoderm: Bencomo et al., 2021. Crustacean decapod: Aguilera et al., 2013; Lima et al., 2023; Fishes: Aguilera et al., 2017a, 2017b).

The analyses of the mineral characterization of carbonate rock conducted in Ilha de Fortaleza (Ponta do Castelo and Fazenda outcrops) were compared to those of reference samples from the outcrops and quarry of the Pirabas Formation, including the following locations: i) Praia do Atalaia, ii) Aricuru, iii) Praia do Maçarico, iv) Baunilha Grande, v) Colônia Pedro Teixeira, and vi) Capanema quarry B-17 (Aguilera et al., 2022). For the mineral characterization (XRD) analyses, all samples were pulverized in a stainless-steel ball mill (SOLAB model SL 38) for 10 min to form fine particles, and subsequently packed into a specific acrylic sample holder fixed in the Spinner system for analysis. The equipment and instrumental conditions were as follows: D2 Phaser XRD Bruker; voltage 30 of kV; amperage of 10 mA; slit 0.6 mm; filter KB Ni; rotation of 15 rpm; measurement time of 0.5 s; starting angle of 10°; angular increases of 0.02°. Phase identification and semiquantitative graphics (DIFFRAC EVAtm Bruker) were used.

For elemental quantification (XRF), a D2 Phaser XRD Bruker was used. All pulverized samples were mixed with lithium tetraborate and funded. The quantitative analyses were calibrated with a certified standard (CAC-2 Calcite) and performed using a Malven Panalytical X-ray fluorescence spectrometer (model Zetium). The ignition losses were performed at 1020 °C for 2 h. Quantitative analyses in carbonate rock over the detection level included percentages of CaO, MgO, $SiO_2$, $Al_2O_3$, $Fe_2O_3$, $Na_2O$, $K_2O$, $P_2O_5$, $TiO_2$, SrO, MnO, and S. The pyrite concretion previously recognized from the Atalaia outcrop (Aguilera et al., 2020a) was analyzed separately in pressed samples following the semi-quantitative method without a standard chemistry pattern (Standardless STD-1) between fluoride and uranium to improve the facies and paleo-environment characterization by integrating outcrops and quarry.

Principal component analysis (PCA) was applied to the XRF results from the analyzed outcrops using the PAST version 3.20 (Hammer et al., 2001). We removed from the analyses $Na_2O$, $K_2O$, $P_2O^5$, $TiO_2$, SrO, MnO, and S which have occurred most of the time in concentrations less than 0.10%. Data were statistically treated by hierarchical cluster analysis and non-metric multidimensional scaling ordination (MDS) based on the Bray-Curtis similarity with PAST version 3.20 (Hammer et al., 2001). We use a SiO2–CaO–FeO3 and Mg–CaO–Al2O3 ternary diagrams to illustrate major element geochemistry of analyzed outcrops.

The rock samples were stored in the Paleoecology and Global Changes Laboratory of Fluminense Federal University, while the macrofossils were donated to the paleontological collection of the Museu de Ciências da Terra, Serviço Geológico do Brasil. Reference collections of macrofossils from the Pirabas Formations deposited in the paleontological repositories of Museu de Ciências da Terra at the Serviço Geológico do Brasil, Museu de Geologia da Universidade Federal do Rio de Janeiro, and Museu Paraense Emílio Goeldi were examined for taxonomy base-line and comparative purposes.

## 4. Results

### 4.1. Lithology

The outcropping successions of Ponta do Castelo and Fazenda are located in the coastal margin, 3.4 km apart and exposed during the lowest tidal regime. The rock surfaces are usually altered by diageneses, hindering the analysis, particularly in the most basal sections (Fig. 2).

The lithologies were observed in the Ponta do Castelo outcrop (Fig. 3A). These included, from the base to the top: i) basal dark-colored to light gray rock (mainly ankerite), 2.0 m thick, massif, without preserved macrofossils on the rock surface or in the matrix; ii) fossiliferous light gray-colored wackestone, 0.47 m thick, grain-supported rocks, containing many molds of dissolved mollusk shells, corals, and broken test and spines of echinoderms in random arrangement; iii) dark-colored and massive packstone, 1.0 m thick, containing many shells, echinoderms, corals, and well preserved shark teeth and tooth plates of rays in random arrangement; iv) yellow colored wackestone, 0.75 m thick, bioturbated with large-size and dense networks of *Thalassinoides* and *Gyrolithes* ichnofossils; v) light gray-colored wackestone, 0.2 m thick, containing many echinoids. The lithology trend is characterized by packstone to grainstone, and fine sand (0.25–0.125 mm).

The lithologies at the Fazenda outcrop (Fig. 3B) comprise from the base to the top: i) light-gray colored mixed massif siliciclastic-carbonate

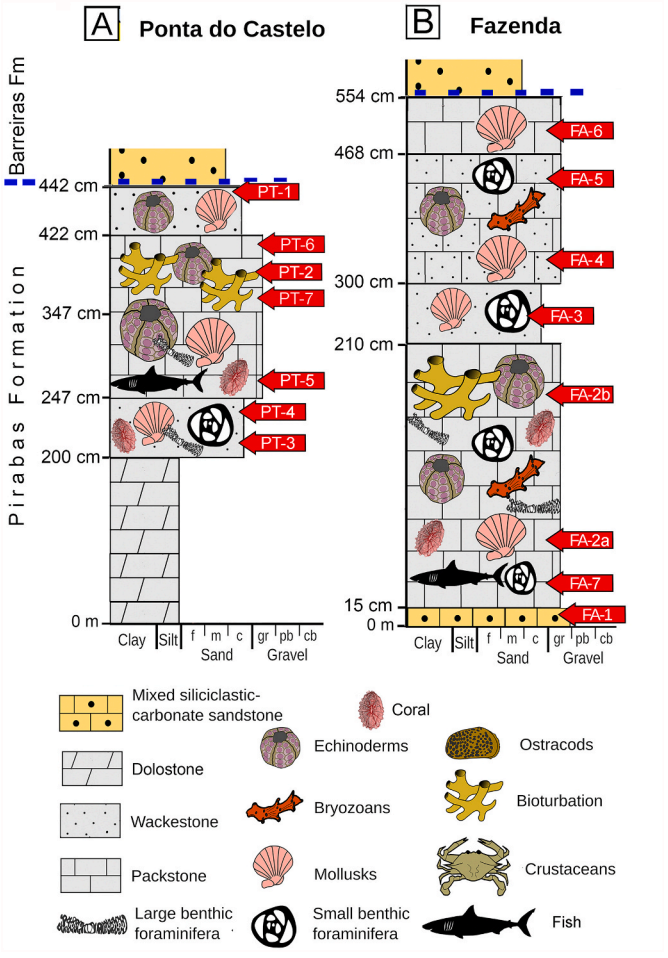


**Fig. 3.** A and B, simplified stratigraphic logs from the Ponta do Castelo and Fazenda respectively (modified from Aguilera et al., 2022). Red arrow = sample label.

sandstone, 0.15 m thick, coarse-grained, with microfossil contents (e.g., Foraminifera, *Pyrgo*); ii) fossiliferous dark-colored and massive packstone, 1.94 m thick, containing many shell molds, echinoderms, corals, bryozoans, and well-preserved shark teeth, all of them in a random arrangement. In addition, *Thalassinoides* ichnofossils with well-lithified burrow walls and empty main channels were recorded in this section; iii) light gray-colored wackestone, 0.90 m thick, characterized by large coarse-grained spheroid nodules; iv) light gray to dark brown-colored packstone/wackestone, 1.68 m thick, containing shell and echinoderm molds and large spheroid nodules-like shapes; v) dark brown-colored packstone, 0.86 m thick, at the top of the section overlayer by the base of the Barreiras Formation. The lithology trend is characterized by very fine sand (0.125–0.062 mm).

### 4.2. Microfossil assemblage

A high concentration and diversity of microfossils, bioclast remains, and grains were recorded in the thin petrography. The bioclast

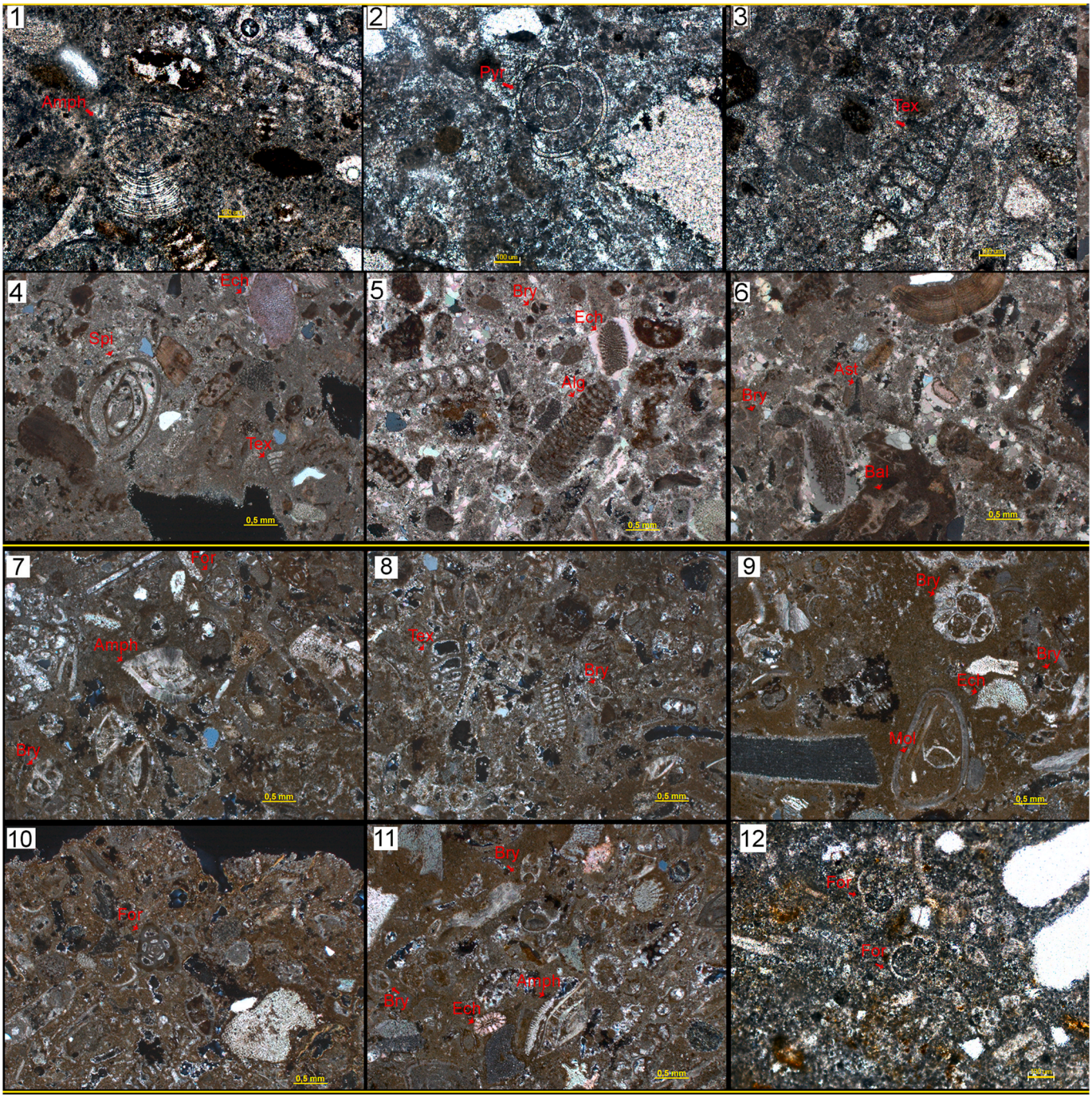


**Fig. 4.** Microphotograph of microfossils at petrography thin from Ilha de Fortaleza (Ponta do Castelo and Fazenda outcrops), São João de Pirabas, Pará State, Brazil. The Ponta do Castelo outcrop comprises: 1, Amphisteginidae (*Amphistegina*) (Amph); 2, Hauerinidae (*Pyrgo*) (Pyr); 3, Textulariidae (*Textularia*) (Tex); 4, Spiroloculinadae (*Spiroloculina*) (Spi) and Textulariidae (*Textularia*) (Tex); 5, coralline algae (Alg), bryozoan (Bry), and echinoids spines of Cidaridae (Ech); 6, asteroid paxila (Ast), bryozoan (Bry), and balanid (Bal). The Fazenda outcrop comprises: 7, Amphisteginidae (*Amphistegina*) (Amph) and bryozoan (Bry); 8, Textulariidae (*Textularia*) (Tex) and bryozoan (Bry); 9, ophiuroids ossicles of Gorgonocephalidae (Ech), Margarettidae (aff. *Margaretta*) (Bry), and bivalve (Mol) 10, planktonic foraminifera (For); 11, Amphisteginidae (*Amphistegina*) (Amph) and Quadricellariidae (aff. *Nellia*) (Bry); 12, *Globorotalia/Globigerina* (For).

components comprise mainly fragments of echinoderms, bryozoans, and mollusks, followed by small and large benthic foraminifera, red and green calcareous algae, ostracods, and barnacles (Table S1). Echinoderms are mostly represented by fragments of echinoid spines from Cidaridae, and ophiuroid ossicles from Gorgonocephalidae. Bryozoans comprise fragments of erect colonies of Candidae, Margarettidae, and Jaculinidae. Mollusks comprise fragments of unidentified bivalves. Benthic foraminifera include Spiroloculinadae, Textulariidae, Amphisteginidae, unidentified small foraminifera, while planktonic foraminifera include Globigerinidae (Fig. 4).

The assemblages of benthic and planktonic foraminifera from disaggregated rocks (Fig. 5) comprise shallow water rotaliid of Amphistegenidae (*Amphistegina*), Elphidiinae (*Elphidium*), Cibicididae (*Cibicides*), and Discorbidae (*Discorbis*), which inhabit coralline algae and coral reefs. Nearshore and lagoon foraminifera are represented by miliolids and comprise Hauerinidae (*Pyrgo* and *Quinqueloculina*) and Soritidae (*Archaias*). Shallow water to open ocean species, including the lagenids, comprise Lagenidae (*Lagena*) and Ellipsolagenidae (*Oolina*), and neritic to pelagic planktonic included Globigerinidae (*Globigerina, Globigerinella, Globigerinoides*, and *Globoturborotalita*). The ostracods (Fig. 6) comprise Cytherellidae, Bairdiidae, Pontocyprididae, Bythocytheridae, Xestoleberididae, Cushmanideidae, Cytheruridae, Cytheridae, Cytherettidae, Hemicytheridae, and Trachyleberididae that inhabit the inner and mid-outer shelfs. Bryozoans include Bugolidae (*Bugula*),

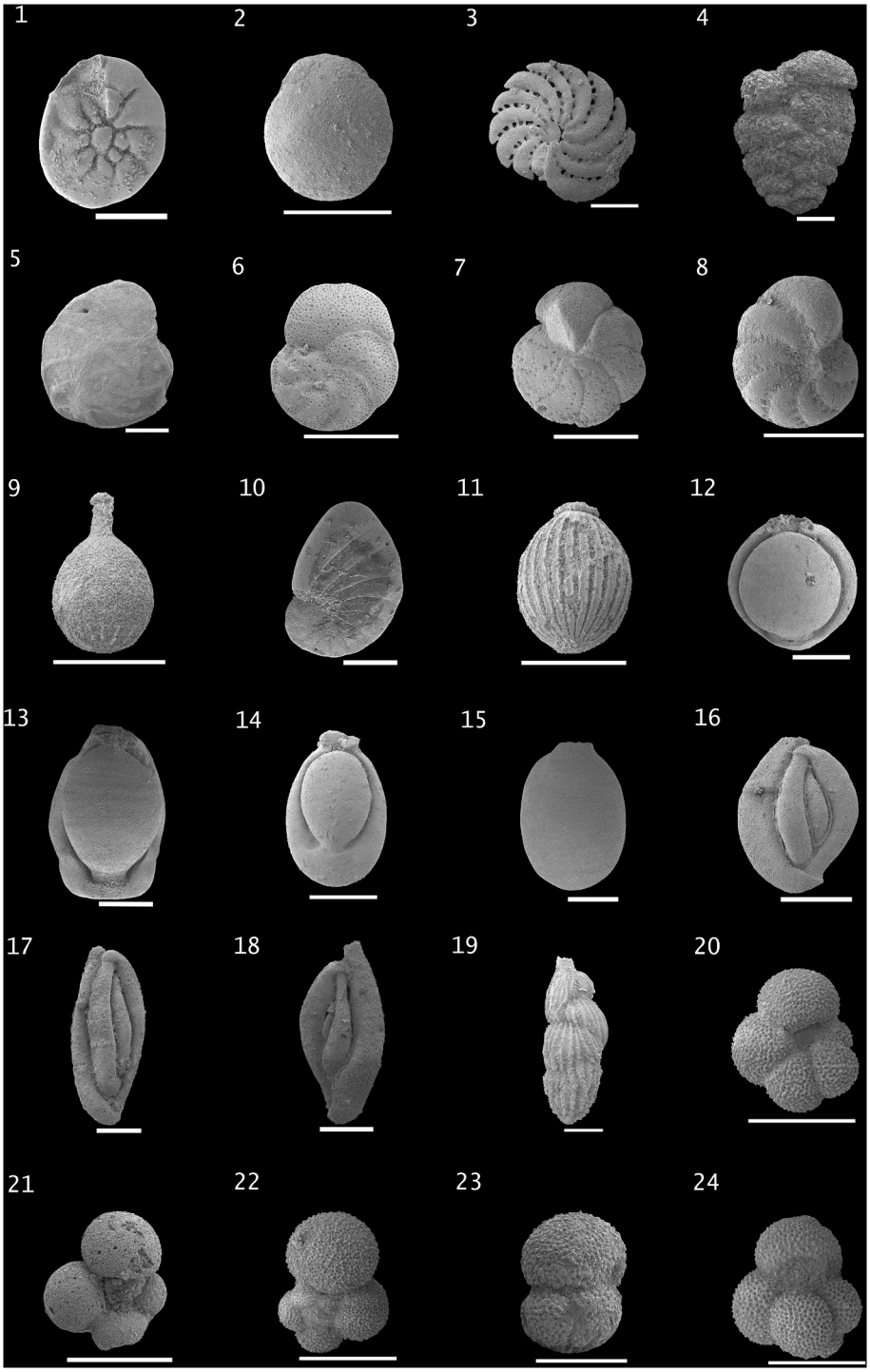


**Fig. 5.** SEM images of Foraminifera species diversity from the Ilha de Fortaleza (Ponta do Castelo and Fazenda outcrops), São João de Pirabas, Pará State, Brazil. Note the mixture of planktonic and benthic Foraminifera in the reworking sediment on shallow water. 1. *Ammonia beccarii*; 2. *Amphistegina lessonii*; 3. *Archaias angulatus*; 4. *Bolivina* sp.; 5. *Cibicides* sp.; 6. *Cibicidoides wuellerstorfi*; 7. ?*Discorbis* sp.; 8. *Elphidium poeyanum*; 9. *Lagena* cf. *Perlucida*; 10. *Nonioella pirabensis*; 11. *Oolina* sp.; 12. *Pyrgo depressa*; 13. *Pyrgo* cf. *Inornata*; 14. *Pyrgo subsphaerica*; 15. *Pyrgo* sp.; 16. *Quinqueloculina lamarckiana*; 17. *Quinqueloculina* sp.; 18. *Triloculina* sp.; 19. *Uvigerina peregrina*; 20. *Globigerina bulloides*; 21. *Globigerina* sp.; 22. *Globigerinella* sp.; 23. *Globigerinoides subquadratus*; 24. *Globoturborotalita* sp. Scale bar: 200 μm.

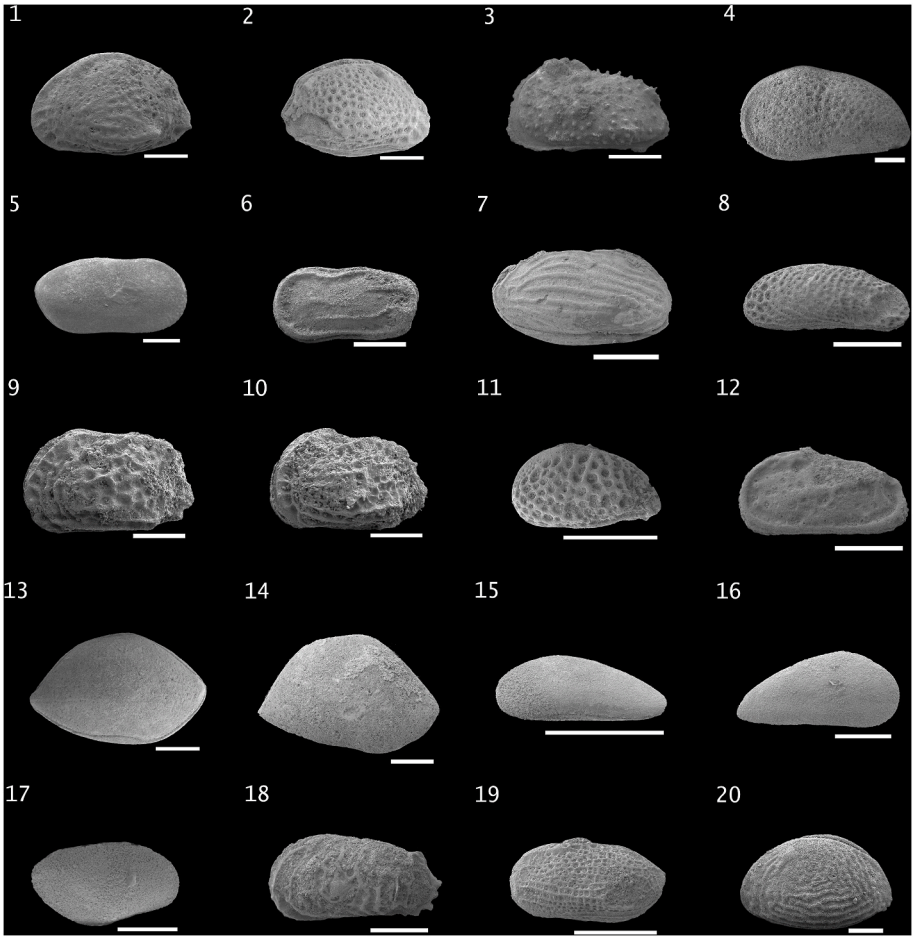


**Fig. 6.** SEM images of ostracod species diversity from the Ilha de Fortaleza (Ponta do Castelo and Fazenda outcrops), São João de Pirabas, Pará State, Brazil. 1. *Aurila amygdala*, LV; 2. *Aurila* cf. *Cicatricosa*, RV; 3. ? *Cativella* sp., LV; 4. ?*Cytheridea* sp., LV; 5. *Cytherella* cf. *Notossinuosa*, RV; 6. *Cytherelloidea mediocythara*, LV; 7. *Cytheretta* cf. *Punctata*, RV; 8. *Cushmanidea* sp., LV; 9. *Quadracythere* sp. 1, LV; 10. *Quadracythere* sp. 2, LV; 11. *Gangamocytheridea* sp., LV; 12. *Neocaudites* sp., LV; 13 *Neonesidea amygdaloides*, RV; 14. *Neonesidea* sp., RV; 15. *Paracypris* sp., LV; 16. *Propontocypris* sp., RV; 17. *Pellucistoma* ?*magniventra*, RV; 18. *Puriana rugipunctata*, LV; 19. *Semicytherura* sp., LV; 20. *Xestoleberis* ?*dactylotypa*, LV. Scale bar: 200 μm. RV: Right Valve. LV: Left Valve.

Jaculinidae (*Pirabasoporella*), Lapaliellidae (*Celleporaria*), Pasytheidae (*Pasythea*), Quadricelleriidae (*Nellia*), Skyloniidae (*Skylonia*), Catenicellidae (*Catenicella* and B*othosella*), and Crissidae (Fig. 7).

### 4.3. Macrofossil assemblage

Macrofossil-rich beds from both the Ponta do Castelo and Fazenda outcrops (Fig. 7, S2) exhibited reworking-associated assemblages dominated by mollusks, echinoderms, bryozoans, ahermatypic corals, crabs, fish, and reptiles (Table S1). The high diversity of mollusk assemblages included bivalve species of Arcidae, Chamidae, Calyptraeidae, Glycymerididae, Ostreidae, Carditidae, Veneridae, Tellinidae, Semelidae, Cardiidae, and Solenidae, most of which have disarticulate valves, broken shells, or molds. The gastropods comprised Olividae, Buccinidae, Melongenidae, Marginellidae, Volutidae, Turbinellidae, Muricidae, Harpidae, Fasciolariidae, Turridae, Columbellidae, Conidae, Terebridae, Strombidae, Thersiteidae, Ficidae, Naticidae, Cypraeidae, Vermetidae, Calyptraedae, Xenophoridae, Renellidae, Cassidae, Turritellidae, Cerithiidae, Architectonicidae, and Fissurellidae, most of which are preserved in a chaotic arrangement compared to the epifauna living position on the seafloor or the infauna natural body axis.

The Ponta do Castelo mollusk assemblage at the base of packstone/wackestone is characterized by mollusk fauna typical of sandy coastlines, which are found at depths of 10–20 m. The assemblages comprised the bivalves *Trachycardium* sp., *Dallocardia* sp. (Cardiidae), *Tellina* sp. (Tellinidae), and gastropods *Marginella* sp. (Marginellidae) and *Natica* sp. (Naticidae). Other groups of sessile mollusks, such as *Crucibulum* sp. (Calyptraedae), and *Arcinella* sp. (Chamidae), are associated with hard substrates, including large shells, so it is not unusual to find them in these sediments. The tops of both outcrops (Fazenda and Ponta do Castelo) show a mixture of mollusks and associated fauna in random positions and/or orientations and come from different habitats. Mollusks inhabit seagrasses (Cerithiidae, Cassidae, and Strombidae), mangroves (Ranellidae, Melongenidae, Arcidae, and Veneridae), rocky environments (Turridae, Fissurellidae, Calyptraeidae, and Conidae), and sandy bottoms (Naticidae, Volutidae, Marginellidae, and Olividae), while others inhabit deeper waters (Xenophoridae, Ficidae, Architectonicidae, Cassidae, and Turritellidae). This is diverse and complex fauna that today would only be found alive in its respective habitats and not mixed like this at the carbonate-siliciclastic rocks.

The echinoderm assemblages are embedded into the massif to coarse-grained packstone/wackestone and consist of poorly preserved echinoid or broken tests and/or isolated spines of Abertellidae, Cassidulidae, Clypeasteridae, Cidaridae, and Echinolampadidae species, as well as, crinoid ossicles of Cormatulidae species. The chaotic arrangement of test fragments, disarticulate spines, and ossicles of both infaunal and epifaunal species was recovered from both sections. Cheilostome bryozoans comprise species of Cupuladriidae and Lepraliellidae embedded in carbonate rock in a chaotic arrangement. The ahermatypic coral Flabellidae comprises isolated specimens that are dispersed into the rock matrix, mostly without a life position. Crustacean decapods comprise Aethridae, Callapidae, Leucosiidae, and Portunidae, recorded by poorly preserved carapaces and disarticulate pereopods. Elasmobranch fishes are represented by well-preserved isolated shark teeth of the coastal-pelagic species of Carcharhinidae, the extinct giant white shark Otodontidae, and the disarticulate tooth plate of the demersal stingray Rhinopteridae. Teleostean fishes comprise the skeletal remains of the demersal porcupinefish Diodontidae. Reptiles comprise long-snouted Crocodylia (Gavialoidea), which are represented by a single isolated tooth.

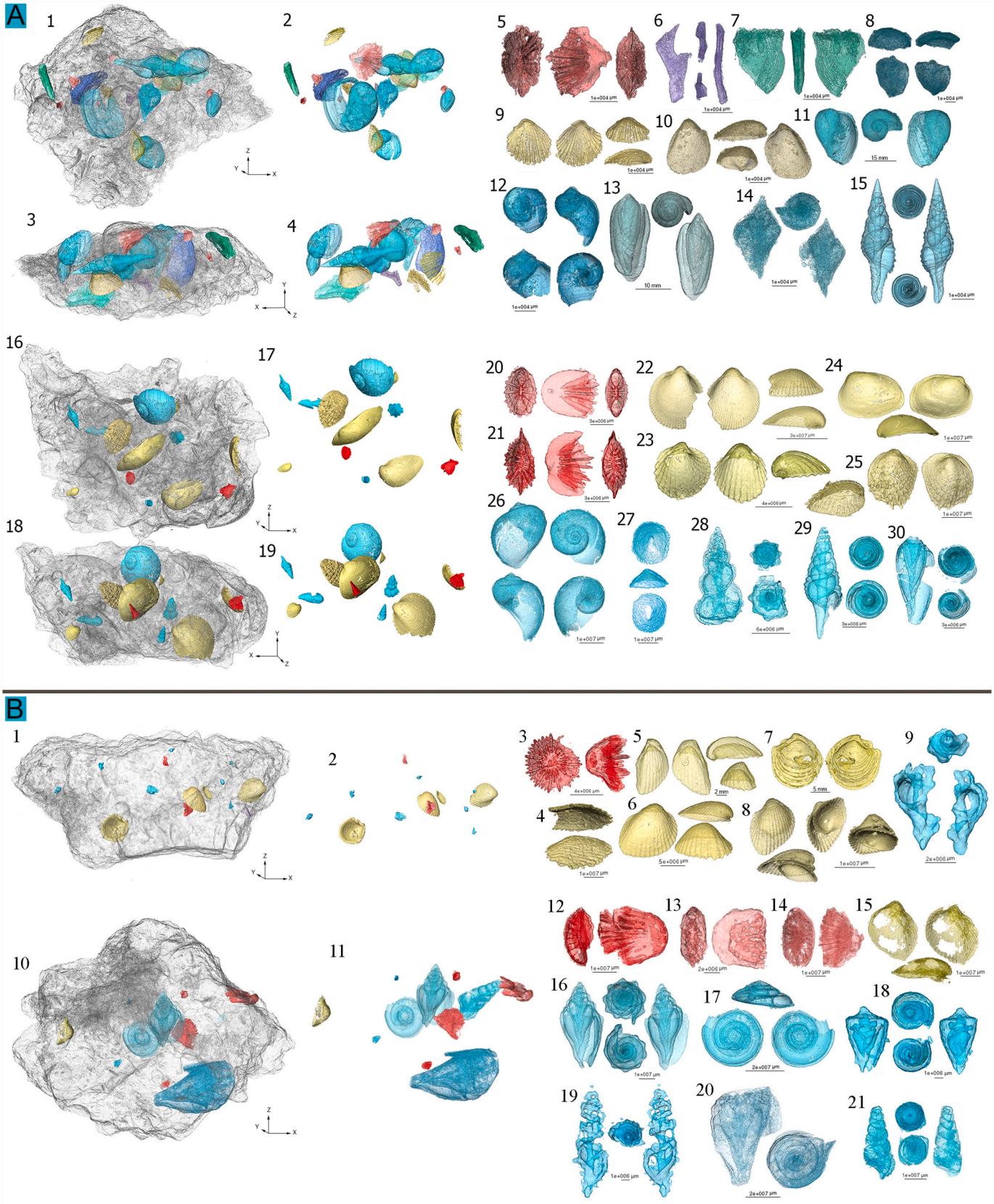


*(caption on next page)*

**Fig. 7.** A. MicroCT images of rock from the Ponta de Castelo outcrop. 1–15, Packstone (PT-5); 1–2, high-resolution volumetry of macrofossil contents in the original plane and vector orientation in the dorsal view of the rock; 3–4, volumetry of macrofossil contents in the original plane and vector orientation in the lateral view of the rock; 5–15, microCT individual 3D reconstruction of specimens in rotating views. 5, Flabellidae ahermatypic coral; 6, Steginoporellidae bryozoan; 7, *Clypeaster* fragment; 8, unidentified; 9, Carditidae; 10, Candiidae; 11, Bullidae; 12, Naticidae; 13, Marginellidae; 14, Strombidae; 15, Turridae. 16–30, Wackestone (PT-3). 16–17, macro fossil contents in the original plane and vector orientation in dorsal view of the rock; 18–19, volumetry of macrofossil contents in the original plane and vector orientation in lateral view of the rock; 20–30, microCT individual 3D reconstruction of specimens in rotating views. 20, 21, Flabellidae ahermatypic coral; 22, Cardiidae, *Cardium* sp.; 23, Cardiidae, *Dallocardia* sp.; 24, Arcidae; 25, Chamidae, *Arcinella* sp; 26, Naticidae, *Natica* sp.; 27, Fasciolariidae, *Fusinus* sp.; 28, Calyptraeidae, *Crucibulum* sp.; 29, Turridae, *Polystira* sp.; 30, Marginellidae, *Marginella* sp. B. MicroCT images of rock from the Fazenda outcrop. 1–9, packstone/wackestone (FA-2b). 2, high-resolution volumetry of macrofossil contents in the original plane and vector orientation in lateral view of the rock (Y axis); 3–9, microCT individual 3D reconstruction of specimens in rotating views. 3, Flabellidae (*Flabellus* sp.); 4, Cupuladridae (*Cupuladria* sp.); 5, Cardiidae (*Dinocardium* sp.); 6, Cardiidae; 7, Lucidae (*Lucina* sp.); 8, Arcidae (*Arca* sp.); 9, Cymatiidae. 10–21, packstone/wackestone (FA-2a). 11, high-resolution volumetry of macrofossil contents in the original plane and vector orientation in lateral view of the rock (Y axis); 12–21, microCT individual 3D reconstruction of specimens in rotating views. 12–14, Flabellidae (*Flabellus* sp.); 15, Arcidae; 16, Volutidae (*Voluta* cf. *caligona*); 17, Architectonidae (*Arquitectonica* cf. *nobilis*); 18, Conidae (*Conus* sp.); 19, 20, Turridae; 21, unidentified gastropod.

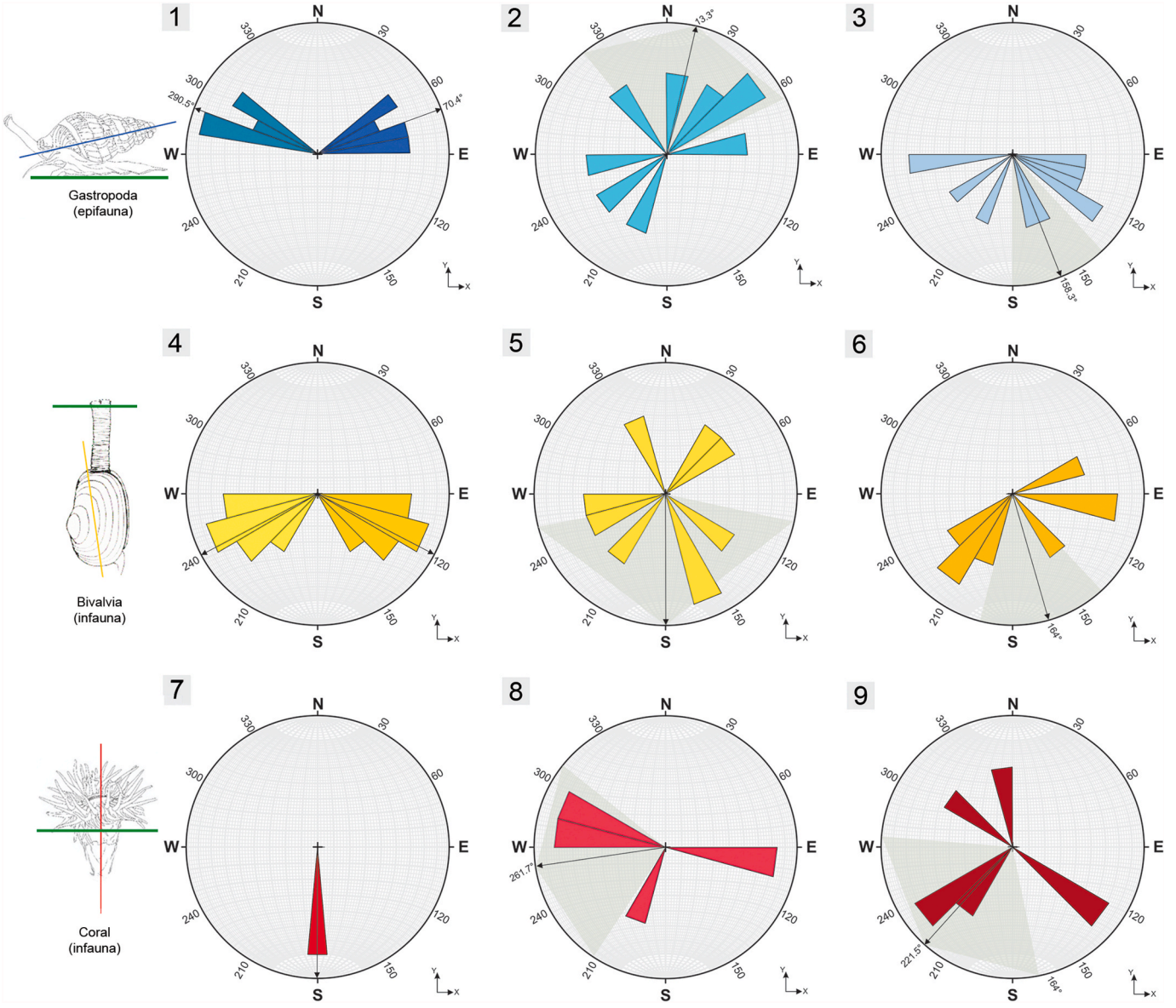


**Fig. 8.** Rose diagram/circular histogram. 1, Reference of living gastropods: left: mean vector = 290.5° ± 4.7°, right mean vector = 70.4° ± 4.3°. 2, Fazenda gastropods: mean vector = 13.3° ± 10.1°. 3, Ponta do Castelo gastropods: mean vector = 158.3° ± 21.5°. 4, Reference of living bivalves: left: mean vector = 242.2° ± 5.0°, mean vector = 117.2° ± 5.0°. 5, Fazenda bivalve: mean vector = 179.7° ± 77.4°. 6, Ponta do Castelo bivalves: mean vector = 164° ± 26.5°. 7, Reference of living corals: mean vector = 180.0° ± 0.5°. 8, Fazenda coral: mean vector = 261.7° ± 47.4°. 9, Ponta do Castelo coral: mean vector = 221.5° ± 53.3°. The schematic draw represents gastropod epifauna, bivalve infauna, and coral infauna. The axis through the shell (blue and yellow lines) and in the coral (red line) are the main axes in the living position to respect the seafloor (green line).

### 4.4. Rose diagram and circular histogram orientation of the Y axis

The fidelity of the angular model and body axis prevalence of the main fossil groups (the Y axis) versus the substrate in relation to the living counterpart arrangement of gastropod and bivalve shells, and coral showed random divergences, giving a chaotic appearance to the set of fossil assemblages in the rock matrix (epifauna or infauna). The microCT analysis, rose diagram, and circular histogram (Fig. 8, Table S2) follow the life position Y axis showing the average angles according to the examined assemblages. Based on the Fazenda rock, the mean gastropods shells vector was 13.3° ± 10.1°, whereas the mean vector of Ponta do Castelo shells was 158.3° ± 21.5°. The mean bivalve shells vector on the Fazenda was 179.7° ± 77.4°, and that from Ponta do Castelo was 164° ± 26.5°. 7. The mean ahermatypic coral vector on the Fazenda was 261.7° ± 47.4°, and that from Ponta do Castelo was 221.5° ± 53.3°.

### 4.5. Porosity

The highest frequency of pore sizes from both outcrops at Ilha de Fortaleza was between 0.01 mm and 0.33 mm reaching 80–90% in terms of pore size distribution (Fig. 9). The mean total porosity was 11.7% (10.6% at the Fazenda and 13.8% at Ponta do Castelo outcrops). This high porosity consisted mainly of: i) the mixed siliciclastic and carbonate sandstone (Fazenda) and ii) plenty of packstone on macrofossils and bioclasts (Ponta do Castelo) (Fig. 10).

### 4.6. Mineral characterization (XRD)

The mineralogical composition (Fig. 10, S5, S6; Table S3) of the oldest outcrops (late early Miocene, 16 Ma) from the Ilha de Fortaleza sections (Ponta do Castelo and Fazenda) comprises calcite and ankerite in the most basal layer. Therefore, they are almost pure carbonates and thus represent an exposed part of the Bragantina platform.

Conversely, other referential outcrops (Praia de Atalaia, Praia do Maçarico, and Aricuru) and the quarry B17 (Fig. 11) from the Pirabas Formation are a mixture of siliciclastic-carbonate and thus they are close to the coast.

### 4.7. Element concentrations (XRF)

The element concentrations testify to the fact that Ponta do Castelo

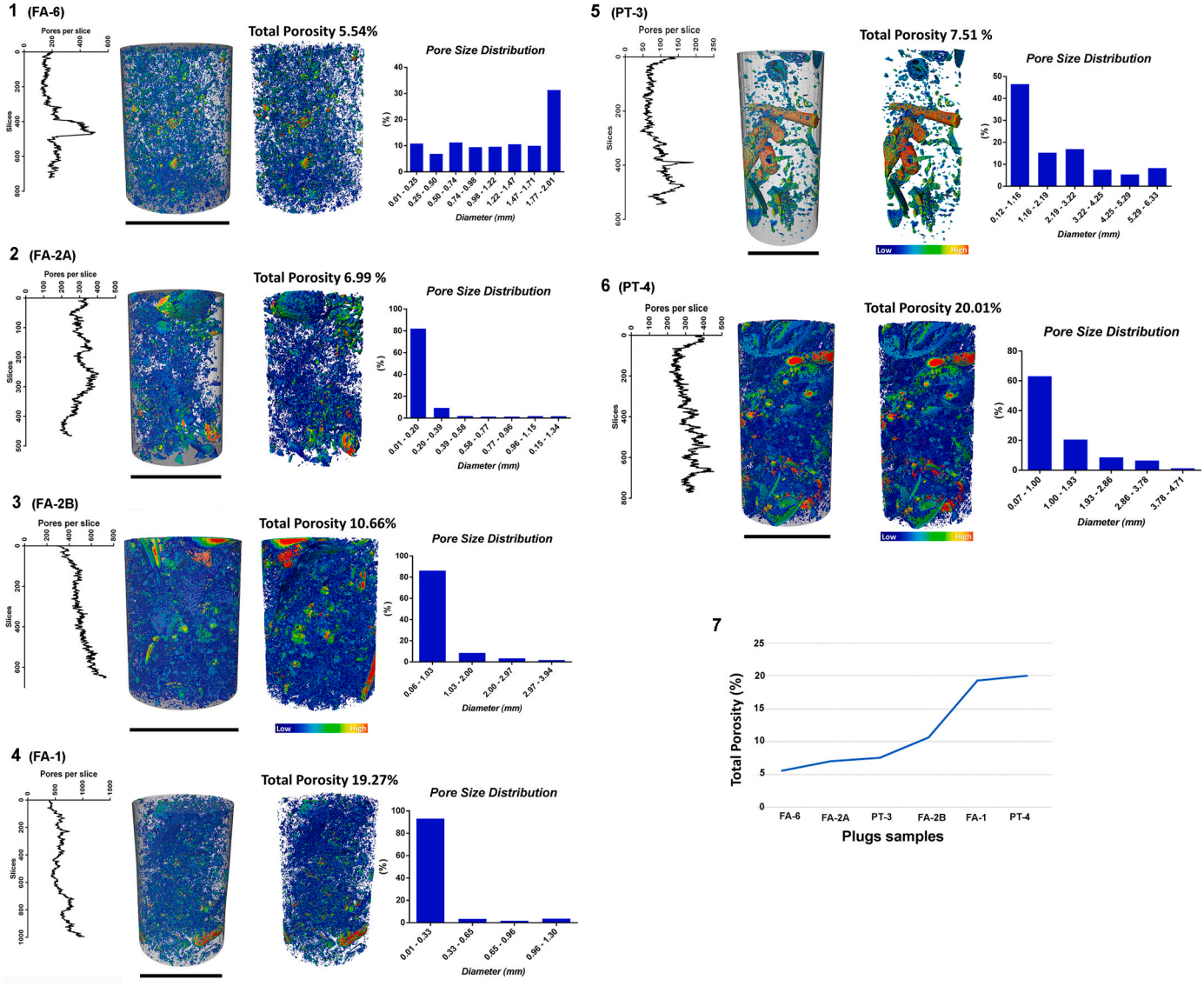


**Fig. 9.** Porosity of carbonate rock at Ilha de Fortaleza from the Fazenda (FA) and Ponta do Castelo (PT) outcrops, showing the diagram of pores per slides, the pore size distribution, the total porosity by plugs, the microCT volumetry and the total porosity of both outcrops included.

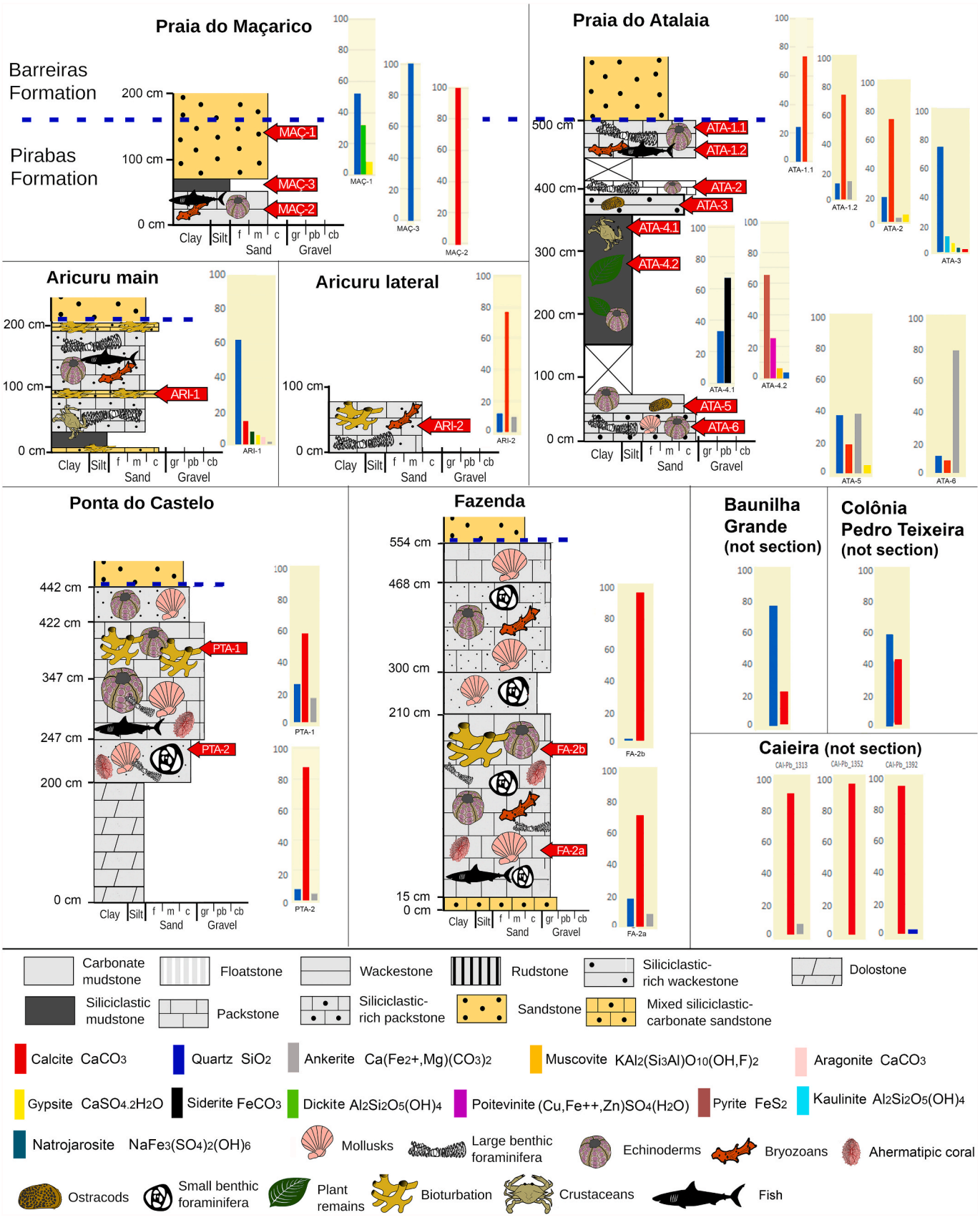


**Fig. 10.** Simplified stratigraphic logs from the Pirabas Formation outcrops and quarry (modified from Aguilera et al., 2022), showing the mineral characterization and the semi-quantitative percent analyzed by X-Ray Diffraction.

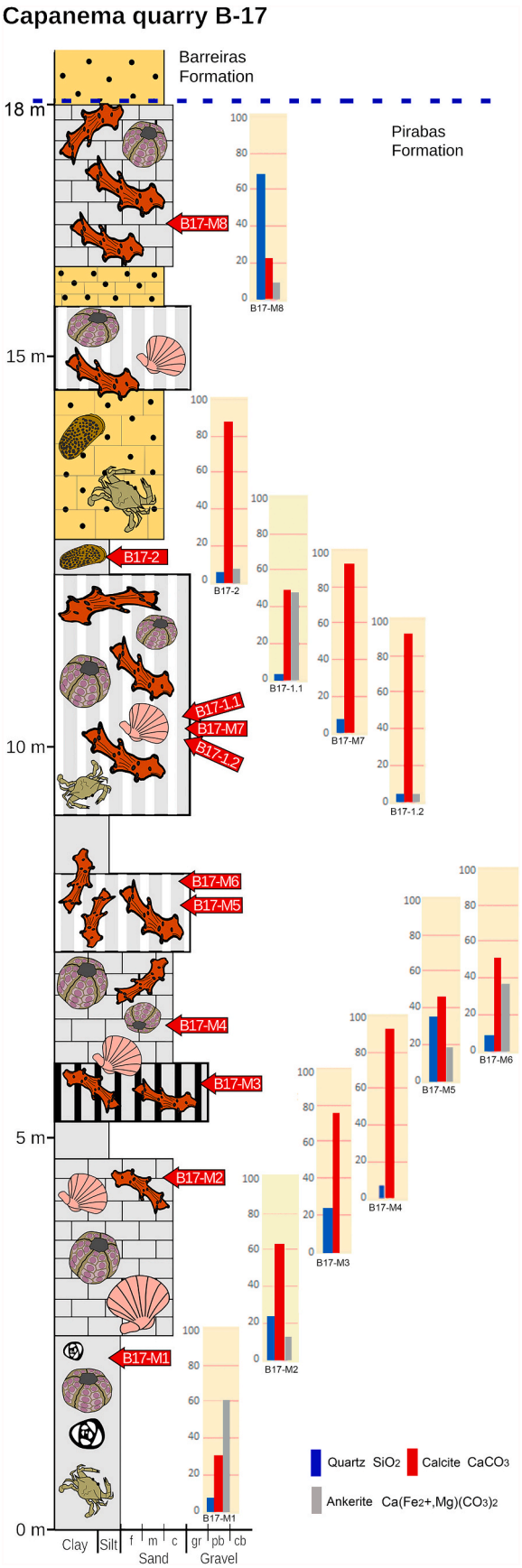


**Fig. 11.** Simplified stratigraphic logs from the Quarry B17 (modified from Aguilera et al., 2022), showing the mineral characterization and the semi-quantitative percent analyzed by X-Ray Diffraction.

and Fazenda represent an exposed part of the platform. The facies α is dominated by CaO (Ponta do Castelo and Fazenda outcrops at Ilha de Fortaleza, and in the referential Capanema B-17 quarry), the facies β shows inputs of terrigenous sources of $SiO_2$, $Al_2O_3$, and $Fe_2O_3$ including other referential outcrops (Praia do Atalaia, Praia do Maçarico, Aricuru, and Baunilha Grande), and the facies *Y* is characterized by MgO involved in the diagenesis processes (basal section of Praia do Atalaia) (Fig. 12, Table S4). Element concentrations (XRF Standardless STD-1) in nodules of pyrite from the redox zone at Praia de Atalaia showed high values of Fe (39.3–41.7%), S (0.72–26.7%), and Si (3.18–2.17%), and were treated separately (Table S5).

## 5. Discussion

### 5.1. Assemblages and bioclasts

The complex of resilient heterozoan species subjected to multiple high-energy waves and oceanic currents could be removed from the bottom and transported during storms, without the collapse of the biotic population. These carbonate constructors produce massive bioclasts during the turnover process, resulting in the accumulation of carbonate substrate for the epifauna and infauna assemblages at the sea beds. Resilience and species turnover characterize the evolutionary realm on the carbonate platform (Foster et al., 2020). Permanent paleoenvironmental changes, such as the establishment of the Amazonas Delta and the input of terrigenous material from the coastal plain drainages, triggered the collapse of the heterozoan carbonate production at the Pirabas Formation in the late Miocene (Aguilera et al., 2022).

### 5.2. Tropical storms

The effects of high-energy storms at the Ponta do Castelo and Fazenda outcrops were recorded in a single stratigraphic sequence, resulting in a high accumulation of fossil fauna mixed in the sediments with a poor stratigraphic context, except in relation to the ground on which the packstone and wackestone rocks are situated over well-consolidated carbonate-siliciclastic sandstone in the Fazenda section and well-consolidated rock of ankerite in Ponta do Castelo. The underlying dark mudstone section below the basal sandstone at Fazenda is currently inaccessible because it is buried by sandy deposits; however, it is described as dark mudstone with pyritized trunks and leaves (Ferreira and Cunha, 1957).

The gentle and shallow slope of the carbonate-siliciclastic inner marine platform of the coastal margin at the Bragantina platform in Pará State, Brazil, the lowland relief of the coastal plain, and the detailed summary of the faunal assemblages from the Ponta do Castelo and Fazenda outcrops testify to the increasing perception of very high category tropical storms, affecting the inner equatorial carbonate-siliciclastic platform of northern Brazil during the Miocene (Fig. 13).

However, the taphonomy effect of shell beds varies substantially depending on the sections of the oceanfront outcrops of the Pirabas Formation and in the paleoenvironment context (Aguilera et al., 2020a, 2020b) and therefore, it is most likely to produce a temporal pattern throughout the composite section, characterizing the three main facies α1, α2, and β (Aguilera et al., 2022). The Ponta do Castelo and Fazenda outcrops from Ilha de Fortaleza are included in facies α, characterized by echinoderm-bryozoan packstone to rudstone rich in mollusks and soritids. Its outcrop was most affected by the older and most oceanfront facies. In this context, the live-dead fidelity model of a transport-induced mixed molluscan assembly (Bhattacherjee et al., 2021) was insufficient for an accurate comparison.

Previous studies in the Neogene biota of tropical America showed a complex pattern of storms affecting shallow-water shell beds at the Miocene Punta Caballo Formation in the Pacific Coast of Costa Rica (Aguilar and Granados, 2018). Currently, hurricanes do not appear to have, to a significant degree, the expected physical effect on coastal

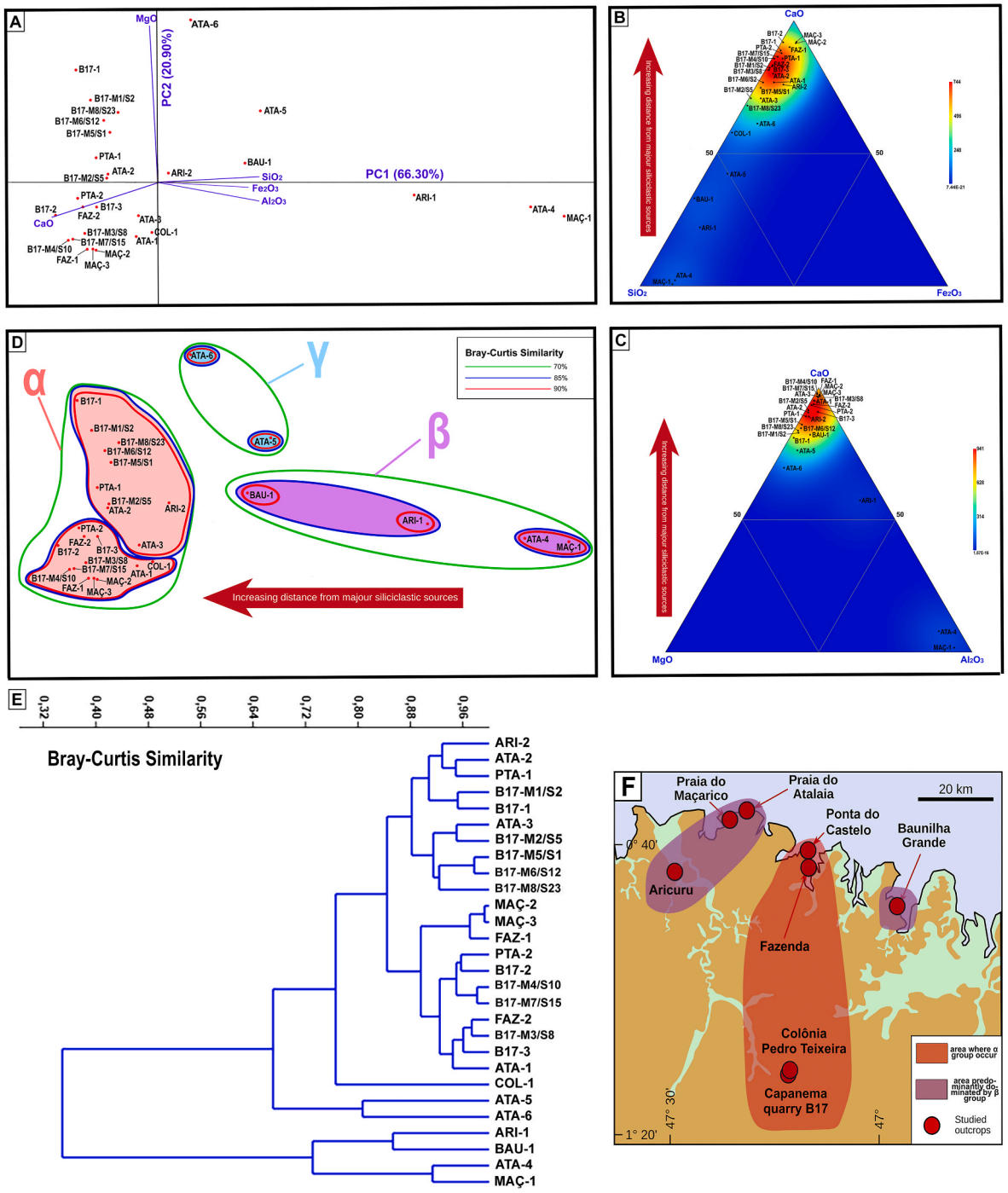


**Fig. 12.** PCA and MDS ordinations and cluster analysis based on elemental ratios by X-Ray Fluorescence (after Log x+1 transformation). A, PCA biplot with the two main PCs. B, C, Ternary diagram illustrating the main major element geochemistry of the analyzed outcrops. D, MDS ordination based on Bray-Curtis similarity displaying the clustering resulting from the cluster analysis of the panel. E, Cluster analysis based on Bray-Curtis similarity. F, Areas predominantly dominated by facies α and β. Abbreviations: B17, Capanema B-17 quarry; PTA, Praia do Atalaia; FAZ, Fazenda; ATA, Praia do Atalaia; ARI, Aricuru; COL, Colônia Pedro Teixeira; BAU, Baunilha Grande; MAÇ, Praia do Maçarico.

benthic fauna, and the potential stress can be mostly attributed to salt-water, low-temperature intrusion, and high anomalous pluviometry precipitation (Engle et al., 2009). However, offshore shallow water reef banks, coral reef islets, and coralline barriers were severely damaged by hurricanes (Bries et al., 2004). Tropical cyclones worldwide generate extreme waves that damage reefs (Puotinen et al., 2020; Dixon et al., 2022).

The inland extension of the carbonatic-siliciclastic rocks from the Pirabas Formation is overlapped by the Barreiras Formation, and it is not accessible to elucidate the final stage of the storm wave incursion towards the mainland. However, referential strata are accessible in quarries such as Caieira in the Municipality of Capanema. The Caieira layers could be the last record of laminar water reflux transporting fine carbonate sediments and dragging leaves of marine-coastal marginal vegetation (Duarte, 2004) along with planktonic foraminifera (Fig. 14) toward calm marine shallow water paleoenvironments.

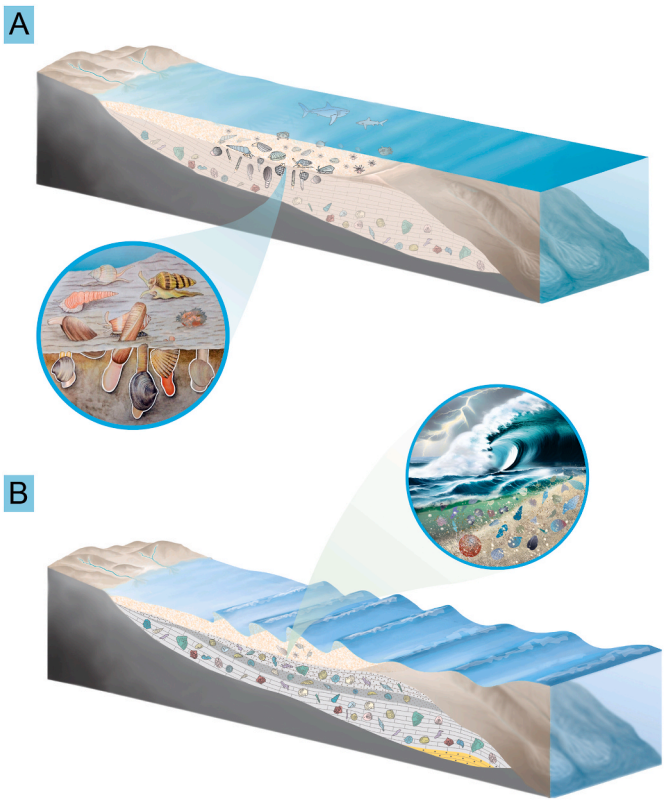


**Fig. 13.** Block diagram and paleoenvironment interpretation. A, Model of shallow water heterozoan assemblage at the middle platform, growing in successive layers and detailed examples of epifauna and infauna in living position. B, Model of shallow water heterozoan assemblage under the influences of storm waves and detailed examples of reworking nekton, plankton, and benthic (epifauna and infauna) faunal assemblages.

### 5.3. Taphonomy

The taphonomic characteristics of the specimens can be interpreted along the spectrum of species ranging from environmentally accumulated reworking assemblages within the habitat to outside the habitat, and the shell assemblage is the result of a chaotic mix of taxa spanning the inner to mid-shelf environments (Fig. 15). The analysis of the morphological characteristics of the shells and tests to evaluate the effects of abrasion, encrustation, bioerosion, and predation (Rahiminejad et al., 2020; Ortiz-Jerónimo et al., 2021) cannot be conclusive because most of them were dissolved, indicating an effect of diagenesis (Pederson et al., 2019) based on the remaining internal molds and shell imprints in the rock matrix. Evidence of disarticulated echinoderms, spines, and ossicles completes the scenario of random faunal assemblages termed storm-dominated carbonate shelf echinoderm taphofacies (Brett et al., 1997). Species/specimens counts are also difficult because most "well-preserved specimens" make up the calcareous rock matrix framework, and the recovery of microCT 3D volumetry is not possible from specimens with X-ray density similar to that of the rock matrix, for example, *Clypeaster*. The probability of accumulating dead shells together with their living counterparts (living-dead fidelity data) at that time could be inaccurate.

Outcrop deposits near the top of the section are characterized by bioturbated wackestone with large and dense networks of well-lithified ichnofossils of *Thalassinoides* and *Gyrolithes*.

According to the registered paleodiversity (Table S1) expressed in the morphology of the shells (mollusk), test, spines, and ossicles (echinoderms), corallum (ahermatypic coral), and skeletons of vertebrates (marine fishes and land reptiles), together with the habitat (infauna or epifauna, pelagic or demersal), burial conditions (live and articulate or died and disarticulate), bottom lithology (mud, sand or gravel), and water flow (energy and directions) result in the complex interpretation of paleocurrent, in the context exhumation, orientation, and transport, for example, modern shell flow experiments (Brenchley and Newwall, 1970; Chattopadhyay et al., 2013) or Miocene shell flow transport (Anderson et al., 2017).

The analysis of the rose diagram and the circular histogram following the Y axis from the Ponta do Castelo and Fazenda outcrops, even separated for taxonomic assemblages (gastropods, bivalves, and ahermatypic corals), showed a high deflection of natural life positions in all examined groups as a consequence of the chaotic arrangement of the benthic community. In addition, the mixture of the exotic hard parts of pelagic/demersal sharks (*Carcharhinus* and *Carcharocles*) and terrestrial/freshwater Crocodylia (Gavialoidea) completes the scenario of mixture and reworking of faunas from the studied outcrops.

The taphonomy should focus on i) the Ponta do Castelo and Fazenda representing an open marine environment; ii) the fossil assemblage includes a mixture of elements from different environments; and iii) the fossil disposition is chaotic. This highlight indicates that they were deposited in a high-energy environment probably battered by storms during the early to middle Miocene on the Pirabas Formation at the coastal margin of the Pará-Maranhão Basin.

### 5.4. Porosity

Carbonate platforms are the most important hydrocarbon reservoirs worldwide, including some world-class hydrocarbon plays, such as the Arab-D Formation in Saudi Arabia, the Asmari Formation in Iran, the Zaedyus field in French Guiana-Suriname, and Perla Limestone in Venezuela (Brownfield and Charpentier, 2006; Wong and van Geuns, 2019; Zalán et al., 2019; De Araújo et al., 2021). Reservoir rocks are characterized by petrophysical properties that favor the storage and fluid flow of hydrocarbons (porosity and permeability). The porosity analysis of the Pirabas Formation at the Praia do Atalaia outcrop (Aguilera et al., 2020a) showed low mean connectivity in the rock matrix (mudstone, 0.97%; dolomudstone, 1.4%; packstone/wackestone, 8.7%). However, at the Aricuru outcrop (Aguilera et al., 2020b; De Araújo et al., 2021) the low connectivity in the rock matrix (packstone/wackestone, 7.5%) contrasts with the high connectivity analyzed in the bioturbations (ichnofossils, 49%). The Ponta do Castelo (Fig. S3) and Fazenda (Fig. S4) outcrops are characterized by bioturbated packstone/wackestone with large and dense networks of well-lithified ichnofossils of *Thalassinoides* and *Gyroliths*. Some of them show a well-developed intraburrow mega porosity, similar to that observed by De Araújo et al. (2021) from the Aricuru outcrop. The connectivity in the rock matrix from both Ponta do Castelo and Fazenda outcrops (mean 11.7% of the total porosity) was higher than that of all other outcrops. Bioturbation improves fluid transmission throughout the sediment by increasing permeability, reducing recharge time, and connecting previously isolated, highly porous layers. In summary, high-energy events can remove fine-grained particles and thus improve the petrographic properties of the rock.

### 5.5. Geochemistry

The mineral characterization and element concentration of Ponta do Castelo and Fazenda outcrop from the Ilha de Fortaleza were dominated by calcite with a high CaO percentage at the facies α, represented by shallow deposits at the inner marine platform with scarce terrigenous influences. Although these marine bottoms were influenced by high-energy wave storms. However, compared to those of reference samples from the outcrops and quarries of the Pirabas Formation the major siliciclastic resources ($Fe_2O$, $SiO_2$, and $Al_2O_3$) and minor calcite proportion were recorded in shallow coastal water facies β.

The Praia do Atalaia section (late middle Miocene, 13–12 Ma) is a

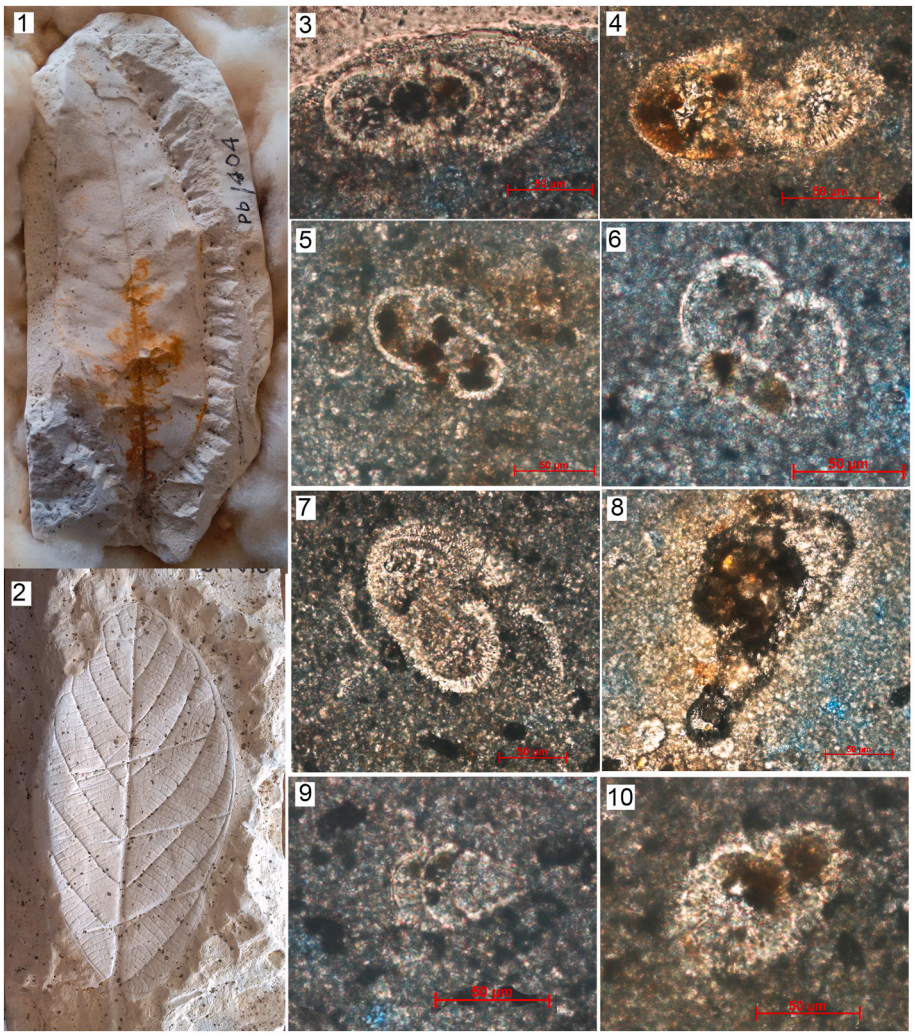


**Fig. 14.** Taphoflora from Caieira leave beds, Capanema municipality, Pirabas Formation and the framework associate Foraminifera. 1, *Guatteria ackermanii*; 2, *Apelba pulchra*; 3–7, *Globorotalia/Globigerina* planktonic foraminifera; 8, microforaminifera linnings; 9, Textulariidae: 10, *Globorotalia/Globigerina*.

model of coastal paleoenvironmental succession at the coastal plain interface, starting with shallow water where the percentage of calcite is replaced by ankerite, followed by the increases of quartz and gypsum; and then, the paleoenvironment changed from a shallow marine to mangrove flood plain characterized by a high percentage of quartz, siderite, pyrite, poitevinite, and muscovite into the redox zone. Finally, at the top of the section, the coastal dynamics change again, and the heterozoan community is re-established, overcropping the mangrove layer or at least with the lesser influence of continental marginal environments.

The Praia do Maçarico and the main Aricuru outcrops (late early Miocene to younger) follows the final phase of the dynamic continental transitional process during the progradation of the Barreiras Formation.

The quarries are characterized by three different highlights: i) the Caieira characterized by laminar reflux transporting fine carbonate sediments with planktonic foraminifera and exotic leaves of coastal vegetation deposited in calm and shallow waters, which is mainly composed of calcite; ii) the Colônia Pedro Teixeira with a percentage of calcite slightly higher than of quartz; and iii) the B17 quarry is characterized by a high proportion of ankerite and calcite at the base; therefore, the percentage of quartz along the section is low, except at the top of the quarry.

Along the modern coast of northern Brazil, bioclastic sediments only occur offshore, near to the coast, where the platform is dominated by terrigenous sediments (Vital et al., 2008; Nascimento et al., 2010; Mahiques et al., 2019). Near the Amazon River mouth, bioclastic sediments occur over 200 km offshore and at a water depth of more than 100 m (Mahiques et al., 2019). Several hundreds of kilometers eastward (e.g., offshore of the state of Ceará), they occur much closer to the coast (60 km or less) and in shallower waters (between 20 m and 70 m) (Vital et al., 2008; Nascimento et al., 2010; Mahiques et al., 2019).

### 5.6. Paleogeography and paleoceanography

There are irrefutable features of the faunal mixture (Fig. 16) and paleoceanographic conditions regarding the southern equatorial platform, which borders the Atlantic-Pacific corridor of the Oligocene–Miocene in the Caribbean and northeastern South America, affecting the boundary of the South American plate and the Panamanian microplate (Coates and Stallard, 2013; Montes et al., 2015; O'Dea et al., 2016; Jaramillo, 2018). Expressive marine shallow water fossiliferous units from the early to middle Miocene, including the Pirabas Formation, could be contextualized in the pre-Panamanian isthmus stage and the interoceanic seaway stage between the Atlantic and Pacific oceans, delimited to the south by the equatorial margin of South America (Fig. 12). Consequently, although the northern coast of Brazil corresponds to a passive continental margin, it is potentially exposed to high-energy storm-derived waves, paleoceanography, and paleoclimatic anomalies.

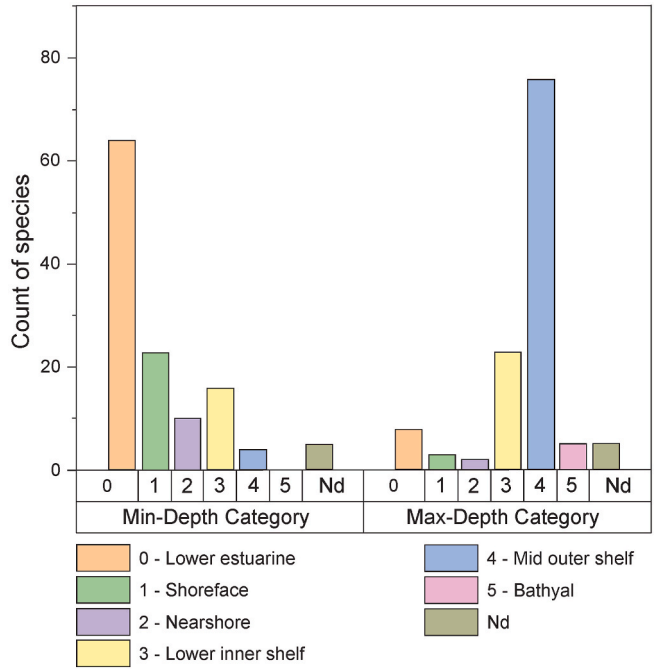


**Fig. 15.** Count of species and the minimal to maximal depth range categories. The data sources are presented in Table S1 except for foraminifera, ostracods, and bryozoans.

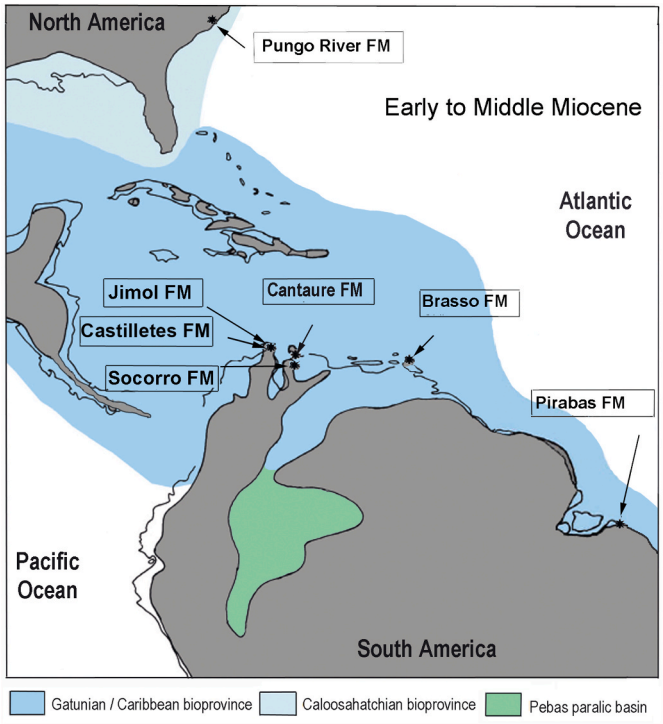


**Fig. 16.** Paleogeographic highlight formations map showing the main marine fossiliferous units from the early to middle Miocene in the context of Neogene Marine Tropical America. Modified schematic reconstruction (Aguilera et al., 2017b).

## 6. Conclusion

1) Ponta do Castelo and Fazenda represent an open marine environment whereas the other referential outcrops are close to the coast; 2) the fossil assemblage includes a mixture of elements from different paleoenvironments; 3) the fossil disposition is chaotic, 4) the high-energy battered by storms during the early to middle Miocene in the Pirabas Formation is conclusive; 5) the resilience and turnover of successive carbonate heterozoan layers took place after each storm episode; and 6) the combination of storm, diagenetic dissolution of hard shells, and ichnofossils are favorable for the development of high porosity and permeability of the carbonate reservoirs.

## Funding

This study was supported by the Brazilian Council of Science and Technological Development - CNPq, Brazil (grant 404937/2018–7 and productivity fellowships 305269/2017–8, 304693/2021–9 to OA); INCT-ANAIS, Brazil (grant 406303/2022–3 and 314225/2021 to RL), and Fundação Carlos Chagas Filho de Amparo à Pesquisa do Estado do Rio de Janeiro - FAPERJ, Brazil (grant E−26/201.035/2021 to OA). DL thanks Fundação Cearense de Apoio ao Desenvolvimento Científico e Tecnológico – FUNCAP, Brazil (grant #PV1-0187-00019.01.00/21 and productivity fellowship BP5-0197-00056.01.00/22).

## Author contributions

O.A., and V.T.K. designed the research. O.A., A.P.L., D.A.S., B.T.G., D.L., and M.C. performed the field research. O.A., O.M.O.A., R.T.L., V.T.K., D.A.S., A.P.L., F.R., and M.C. performed the research. O.A., O.M.O.A., R.T.L., D.A.S., A.P.L., B.T.G., J.S.S., F.R., D.L., and M.C. contributed data. M.M., R.D., H.S.G.F., M.J.D.A., D.L., F.R., and D.A.S. analyzed data. O.A., O.M.O.A., and M.J.G. drafted figures. O.A., V.T.K., O.M.O.A., R.T.L., F.R. A.P.L., and M.C. wrote the paper. All authors performed the manuscript review.

## Declaration of competing interest

The authors declare that they have no known competing financial interests or personal relationships that could have appeared to influence the work reported in this paper.

## Data availability

No data was used for the research described in the article.

## Acknowledgments

The authors would like to thank the National Mining Agency of Brazil; the Brazilian Geological Service; the Federal Fluminense University, the departments of Marine Biology and Environmental Geochemistry; the Federal University of Rio de Janeiro, Nuclear Engineering Program/COPPE; The Rio de Janeiro State University, Department of Applied Physics and Thermodynamics; The Federal University of Pará, Postgraduation Program in Geology and Geochemistry; The Paraense Emilio Goeldi Museum; the Smithsonian Tropical Research Institute. We thank G. Coletti, C. Jaramillo, A.V. de Souza, C. Lamarão, S. Ramos, R. Costa, J. Lobos, C. Nig, H. Costi, A. Soares, and M. Concha for valuable discussion, data, and assistance. Thanks also to Juan Carlos Laya (Associate Editor of JMPG) and anonymous reviewers for their valuable comments that greatly contributed to improving the manuscript.

O. Aguilera and F. Rodriguez acknowledge here a tribute to the advisor and mentor Dr. Anthony G. Coates (1936–2022), Senior Scientist Emeritus at Smithsonian Tropical Research Institute (STR), for his dedication to the study of the geology and paleontology of tropical America.

## Appendix A. Supplementary data

Supplementary data to this article can be found online at https://doi.

org/10.1016/j.marpetgeo.2023.106333.

## References


Abreu, W.S., Regali, M.P.S., Shimabukuro, S., 1986. O Terciário da plataforma continental do Maranhão e Pará, Brasil: bioestratigrafia e evolução paleoambiental. In: Anais do XXXIV Congresso Brasileiro de Geologia, Goiânia, vol. 1, pp. 145–159.

Aguilar, T., Granados, R., 2018. Depósitos someros de acumulación de conchas afectados por tormentas en el Pacífico Central de Costa Rica, Formación Punta Carballo. Mioceno. Rev. Geog. Am. Cent. 59, 61–74. https://doi.org/10.15517/rgac.v59i0.34159.

Aguilera, O., Guimarães, J.T.F., Morães-Santos, H., 2013. Neogene eastern Amazon carbonate platform and the palaeoenvironmental interpretation. Swiss J. Palaeontol. 132, 99–118. https://doi.org/10.1007/s13358-014-0066-6.

Aguilera, O., Luz, Z., Carrillo-Briceño, J.D., Kocsis, L., Vennemann, T.W., Toledo, P.M., Nogueira, A., Amorim, K.B., Moraes-Santos, H., Polck, M.R., Ruivo, M.L., Linhares, A.P., Monteiro-Neto, C., 2017a. Neogene sharks and rays from the Brazilian 'blue Amazon'. PLoS One 12 (8), e0182740. https://doi.org/10.1371/journal.pone.0182740.

Aguilera, O., Silva, G.O.A., Lopes, R.T., Machado, A.S., dos Santos, T.M., Marques, G., Bertucci, T., Aguiar, T., Carrillo-Briceño, J., Rodriguez, F., Jaramillo, C., 2017b. Neogene proto-caribbean porcupinefishes (diodontidae). PLoS One 12, e0181670. https://doi.org/10.1371/journal.pone.0181670.

Aguilera, O., de Araújo, O.M.O., Hendy, A., Nogueira, A.A.E., Nogueira, A.C.R., Maurity, C.W., Kütter, V.T., Martins, M.V.A., Coletti, G., Dias, B.B., Silva-Caminha, S. A.F., Jaramillo, C., Bencomo, K., Lopes, R.T., 2020a. Palaeontological framework from Pirabas Formation (North Brazil) used as potential model for equatorial carbonate platform. Mar. Micropaleontol. 154, 1–23. https://doi.org/10.1016/j.marmicro.2019.101813.

Aguilera, O., Bencomo, K., de Araújo, O.M.O., Dias, B.B., Coletti, G., Lima, D., Silva-Caminha, S.A.F., Polk, M., Martins, M.V.A., Jaramillo, C., Kütter, V.T., Lopes, R.T., 2020b. Miocene heterozoan carbonate systems from the western Atlantic equatorial margin in South America: the Pirabas formation. Sediment. Geol. 407, 1–28. https://doi.org/10.1016/j.sedgeo.2020.105739.

Aguilera, O., Martins, M.V.A., Linhares, A.P., Kütter, V.T., Coletti, G., 2022. Palaeoenvironment of the Miocene Pirabas Formation mixed carbonate–siliciclastic deposits, Northern Brazil: insights from skeletal assemblages. Mar. Petrol. Geol. 145, 105588 https://doi.org/10.1016/j.marpetgeo.2022.105855.

Anderson, B.M., Hendy, A., Johnson, E.H., Allmon, W.D., 2017. Paleoecology and paleoenvironmental implications of turritelline gastropod-dominated assemblages from the Gatun Formation (Upper Miocene) of Panama. Palaeogeogr. Palaeoclimatol. Palaeoecol. 470, 132–146. https://doi.org/10.1016/j.palaeo.2017.01.026.

Banha, T.N.S., Luiz, O.J., Asp, N.E., Pinheiro, H.T., Magris, R.A., Cordeiro, R.T.S., Mahiques, M.M., Mies, M., Giglio, V.J., Omachi, C.Y., Siegle, E., Nogueira, L.C., Thompson, C.C., Thompson, F.L., Nora, V., Horta, P.A., Rezende, C.E., Sumida, P.Y. G., Ferreira, C.E.L., Floeter, S.R., Francini-Filho, R.B., 2022. The great Amazon reef system: a fact. Front. Mar. Sci. 9, 1088956 https://doi.org/10.3389/fmars.2022.1088956.

Barrera-Lopez, C.V., Mooney, W.D., Kaban, M.K., 2022. Regional geophysics of the caribbean and northern South America: implications for tectonics. G-cubed 23 (5), e2021GC010112. https://doi.org/10.1029/2021GC010112.

Bencomo, K., Mihaljević, M., De Araújo, O.M., Lopes, R.T., Lima, D., Aguilera, O., 2021. Dominance of Miocene echinoderms in the equatorial Neogene marine platform of Brazil and their insights into the paleoenvironment. J. S. Am. Earth Sci. 112 (1), 103595 https://doi.org/10.1016/j.jsames.2021.103595.

Bhanat, N., Nagori, M.L., Chaudhary, M., 2018. Distribution of ostracod fauna and environment of deposition of early Miocene (Aquitanian-Burdigalian) sediments in Kachchh, Gujarat. Indian J. Appl. Res. 8 (2), 380–382.

Bhattacherjee, M., Chattopadhyay, D., Som, B., Ammu, S., Satyaki, M., 2021. Molluscan live-dead fidelity of a storm-dominated shallow-marine setting and its implications. Palaios 36 (2), 77–93. https://doi.org/10.2110/palo.2020.020.

Brenchley, P.J., Newwall, G., 1970. Flume experiments on the orientation and transport of models and shell valves. Palaeogeogr. Palaeoclimatol. Palaeoecol. 7 (3), 185–220.

Brett, C.E., Moffat, H.A., Taylor, W.L., 1997. Echinoderm taphonomy, taphofacies, and Lagerstätten. Paleontol. Soc. Pap. 3, 147–190. https://doi.org/10.1017/S1089332600000243.

Bries, J.M., Debrot, A.O., Meyer, D.L., 2004. Damage to the leeward reefs of curaçao and bonaire, Netherlands antilles from a rare storm event: hurricane lenny, november 1999. Coral Reefs 23, 297–307. https://doi.org/10.1007/s00338-004-0379-9.

Brownfield, M.E., Charpentier, R.R., 2006. Geology and Total Petroleum Systems of the Gulf of Guinea Province of West Africa, 2207-C. U.S. Geological Survey Bulletin, p. 32. https://doi.org/10.3133/b2207C.

Cairns, S.D., 2016. A key to the genera and species of the transversely-dividing Flabellidae (Anthozoa, Scleractinia, Flabellidae), with a guide to the literature, and the description of two new species. ZooKeys 562, 1–48. https://doi.org/10.3897/zookeys.562.7310.

Cairns, S.D., 2017. New azooxanthellate genus of scleractinia (Flabellidae) from the Australian cenozoic. J. Paleontol. 91 (3), 407–416. https://doi.org/10.1017/jpa.2016.83.

Calvert, S.E., Pedersen, T.F., 2007. Chapter fourteen elemental proxies for palaeoclimatic and palaeoceanographic variability in marine sediments: interpretation and application. Dev. Mar. Geol. 1, 567–644. https://doi.org/10.1016/S1572-5480(07)01019-6.

Cann, J.H., Bourman, R.P., Barnett, E.J., 2000. Holocene foraminifera as indicators of relative estuarine-lagoonal and oceanic influences in estuarine sediments of the river murray, south Australia. Quat. Res. 53 (3), 378–391. https://doi.org/10.1006/qres.2000.2129.

Carannante, G., Esteban, M., Milliman, J.D., Simone, L., 1988. Carbonate lithofacies as paleolatitude indicators: problems and limitations. Sediment. Geol. 60 (1–4), 333–346. https://doi.org/10.1016/0037-0738(88)90128-5.

Chattopadhyay, D., Rathie, A., Das, A., 2013. The effect of morphology on postmortem transportation of bivalves and its taphonomic implications. Palaios. Sediment. Geol. 28, 203–209. https://doi.org/10.2110/palo.2012.p12-103r.

Coates, A.G., Stallard, R.F., 2013. How old is the Isthmus of Panama? Bull. Mar. Sci. 89, 801–813. https://doi.org/10.5343/bms.2012.1076.

Cohen, M.C.L., de Souza, A.V., Liu, K.-B., Rodrigues, E., Yao, Q., Pessenda, L.C.R., Rossetti, D., Ryu, J., Dietz, M., 2021. Effects of beach nourishment project on coastal geomorphology and mangrove dynamics in southern Louisiana, USA. Rem. Sens. 13, 2688. https://doi.org/10.3390/rs13142688.

Cotrim, C.S., Semedo, A., Lemos, G., 2022. Brazil wave climate from a high-resolution wave hindcast. Climate 10 (4), 53. https://doi.org/10.3390/cli10040053.

Cruz, A.M., Reis, A.T., Suc, J.P., Silva, C.G., Praeg, D., Granjeon, D., Rabineau, M., Popescu, S.M., Gorini, C., 2019. Neogene evolution and demise of the Amapá carbonate platform, Amazon continental margin, Brazil. Mar. Petrol. Geol. 105, 185–203. https://doi.org/10.1016/j.marpetgeo.2019.04.009.

De Araújo, O.M.O., Aguilera, O., Coletti, G., Valencia, F.L., Buatois, L.A., Lopes, R., 2021. X-ray micro-computed tomography of burrow-related porosity and permeability in shallow-marine equatorial carbonates: a case study from the Miocene Pirabas Formation. Brazil. Mar. Pet. Geol. 127, 104966 https://doi.org/10.1016/j.marpetgeo.2021.104966.

De Sousa, T.A., Venancio, I.M., Valeriano, C.M., Heilbron, M., Carneiro, M.T.W.D., Mane, M.A., Almeida, J.C.H., Smoak, J.M., Albuquerque, A.L.S., Silva-Filho, E.V., 2021. Changes in sedimentary provenance and climate off the coast of Northeast Brazil since the Last Interglacial. Mar. Geol. 435, 106454 https://doi.org/10.1016/j.margeo.2021.106454.

Dixon, A.M., Puotinen, M., Ramsay, H.A., Beger, M., 2022. Coral reef exposure to damaging tropical cyclone waves in a warming climate. Earth's Future 10 (8), e2021EF002600. https://doi.org/10.1029/2021EF002600.

Duarte, L., 2004. Paleoflórula. In: Rossetti, D.F., Góes, A.M. (Eds.), O Neógeno da Amazônia Oriental. Museu Paraense Emílio Goeldi (Coleção Friederich Katzer), pp. 169–198.

Engle, V.D., Hyland, J.L., Cooksey, C., 2009. Effects of Hurricane Katrina on benthic macroinvertebrate communities along the northern Gulf of Mexico coast. Environ. Monit. Assess. 150, 193–209. https://doi.org/10.1007/s10661-008-0677-8.

Ferreira, C.S., Cunha, O.R., 1957. Contribuição à Paleontologia do estado do Pará. Notas sobre a formação Pirabas, com descrições de novos invertebrados fósseis. I – (Mollusca – gastropoda). Bol. Mus. Para. Emílio Goeldi, Nova Sér., Geologia 2, 1–60.

Figueiredo, J., Hoorn, C., van der Vem, P., Soares, E., 2009. Late Miocene onset of the Amazon River and the Amazon deep-sea fan: evidence from the foz do Amazonas basin. Geology 37 (7), 619–622. https://doi.org/10.1130/G25567A.1.

Forsey, G.F., 2016. Ostracods as proxies for past seagrass: a review. Palaeogeogr. Palaeoclimatol. Palaeoecol. 447, 22–28. https://doi.org/10.1016/j.palaeo.2016.01.028.

Foster, W.J., Garvie, C.L., Weiss, A.M., Muscente, A.D., Aberhan, M., Counts, J.W., Martindale, R.C., 2020. Resilience of marine invertebrate communities during the early Cenozoic hyperthermals. Sci. Rep. 10 https://doi.org/10.1038/s41598-020-58986-5, 2176.

Gebregiorgis, D., Giosan, L., Hathorne, E.C., Anand, P., Nilsson-Kerr, K., Plass, A., Lückge, A., Clemens, S.C., Frank, M., 2020. What can we learn from X-ray fluorescence core scanning data? A paleomonsoon case study. G-cubed 21 (2), e2019GC008414. https://doi.org/10.1029/2019GC008414.

Gomes, B.T., Aguilera, O., Silva-Caminha, S.A.F., D'Apolito, C., Cárdenas, D., Hocking, E. P., Lemes, K.K.B., 2023. Biostratigraphy and paleoenvironments of the Pirabas Formation (Neogene, Pará state-Brazil). Mar. Micropaleontol. 180, 102218 https://doi.org/10.1016/j.marmicro.2023.102218.

Gorini, C., Haq, B.U., Reis, A.T., Silva, C.G., Cruz, A., Soares, E., Grangeon, D., 2014. Late Neogene sequence stratigraphic evolution of the foz do Amazonas basin, Brazil. Terra. Nova 26, 179–185. https://doi.org/10.1111/ter.12083.

Govin, A., Holzwarth, U., Heslop, D., Keeling, L.F., Zabel, M., Mulitza, S., Collins, J.A., Chiessi, C.M., 2012. Distribution of major elements in Atlantic surface sediments (36°N–49°S): imprint of terrigenous input and continental weathering. G-cubed 13 (1), 1–23. https://doi.org/10.1029/2011GC003785.

Guernet, C., Fourcade, E., 1988. Cenozoic ostracodes from hole 628A, ODP leg 101, Bahamas. In: Austin, J.A., Schlager, W., et al. (Eds.), Proceedings of the Ocean Drilling Program, Scientific Results, vol. 101. College Station: Ocean Drilling Program, pp. 139–151. In: https://doi:10.2973/odp.proc.sr.101.123, 1988.

Hammer, Ø., Harper, D.A.T., Ryan, P.D., 2001. Past: paleontological Statistics software package for education and data analysis. Palaeontol. Electron. 4 (1), 1–9.

Haq, B.U., Hardenbol, J., Vail, P.R., 1987. Chronology of fluctuating sea levels since the triassic. Science 235 (4793), 1156–1167. https://doi.org/10.1126/science.235.4793.1156.

Hendy, A.J.W., 2013. Spatial and stratigraphic variation of marine paleoenvironments in the middle-upper Miocene gatun formation, isthmus of Panama. Palaios 28 (4), 210–227. http://www.bioone.org/doi/full/10.2110/palo.2012.p12-024r.

Hendy, A.J.W., Jones, D.S., Moreno, F., Zapata, V., Jaramillo, C., 2015. Neogene molluscs, shallow marine paleoenvironments, and chronostratigraphy of the Guajira Peninsula, Colombia. Swiss J. Palaeontol. 134, 45–75. http://www.bioone.org/doi/10.1007/s13358-015-0074-1.

Herold, N., Huber, M., Müller, R.D., Seton, M., 2012. Modeling the Miocene climatic optimum: ocean circulation. Paleoceanography 27, PA1209. https://doi.org/10.1029/2010PA002041.

Jaramillo, C.A., 2018. Evolution of the isthmus of Panama: biological, paleoceanographic and paleoclimatological implications. In: Hoorn, C., Perrigo, A., Antonelli, A. (Eds.), Mountains, Climate and Biodiversity. Wiley Blackwell, Oxford, pp. 323–338.

Javaux, E.J., Scott, D.B., 2003. Illustration of modern benthic foraminifera from Bermuda and remarks on distribution in other subtropical/tropical areas. Palaeontol. Electron. 6 (4), 1–29. http://palaeo-electronica.org/paleo/, 2003_1/benthic/issue1_03.ht.

Kominz, M.A., Browning, J.V., Miller, K.G., Sugarman, P.J., Mizintseva, S., Scotese, C.R., 2008. Late Cretaceous to Miocene sea-level estimates from the New Jersey and Delaware coastal plain coreholes: an error analysis. Basin Res. 20 (2), 211–226. https://doi.org/10.1111/j.1365-2117.2008.00354.x.

Lima, D., Tavares, M., Lopes, R.T., de Araújo, O.M.O., Aguilera, O., 2020. Uca maracoani (Crustacea, Decapoda, Ocypodidae) from a Miocene paleomangrove in Brazil: a case of evolutionary stasis among tropical American fiddler crabs. J. South Am. Earth Sci. 99, 102517 https://doi.org/10.1016/j.jsames.2020.102517.

Lima, D., da Silva, R.C., Aguilera, O., Pinheiro, A.P., Santana, W., 2023. Brazilian Miocene crabs I. Taxonomic review of cyclocancer tuberculatus beurlen, 1958 and hepatella amazonica beurlen, 1958 (pancrustacea, Decapoda, Brachyura). Pap. Avulsos Zool. (Sao Paulo) 63, e202363012. https://doi.org/10.11606/1807-0205/2023.63.012.

Mahiques, M.M., Siegle, E., Francini-Filho, R.B., Thompson, F.L., de Rezende, C.E., Gomes, J.D., Asp, N.E., 2019. Insights on the evolution of the living great Amazon reef system, equatorial west atlantic. Sci. Rep. 9 (1), 13699 https://doi.org/10.1038/s41598-019-50245-6.

Mateu-Vicens, G., Hallock, P., Brandano, M., 2008. A depositional model and paleoecological reconstruction of the lower Tortonian distally steepened ramp of Menorca (Balearic Islands, Spain). Palaios 23 (7), 465–481. https://doi.org/10.2110/palo.2007.p07-061r.

Maury, C.J., 1925. Fósseis terciários do Brasil com descrição de novas formas Cretáceas, vol. 4. Serviço Geológico e Mineralógico do Brasil, Monografia, 665.

Montes, C., Cardona, A., Jaramillo, C., Pardo, A., Silva, J.C., Valencia, V., Ayala, C., Pérez-Angel, L.C., Rodriguez-Parra, L.A., Ramirez, V., Niño, H., 2015. Middle Miocene closure of the central American seaway. Science 348 (6231), 226–229. https://www.science.org/doi/full/10.1126/science.aaa2815.

Nascimento, F.S., Freire, G.S.S., Miola, B., 2010. Geochemistry of marine sediments of the Brazilian Northeastern continental shelf. Braz. J. Oceanogr. 58 (spe2), 1–11.

O'Dea, A., Lessios, H.A., Coates, A.G., Eytan, R.I., Restrepo-Moreno, S.A., Cione, A.L., Collins, L.S., Queiroz, A., Farris, D.W., Norris, R.D., Stallard, R.F., Woodburne, M.O., Aguilera, O., Aubry, M.-P., Berggren, W.A., Budd, A.F., Cozzuol, M.A., Coppard, S.E., Duque-Caro, H., Finnegan, S., Gasparini, G.M., Grossman, E.L., Johnson, K.G., Keigwin, L.D., Knowton, N., Leigh, E.G., Leonard-Pingel, J.S., Marko, P.B., Pyenson, N.D., Rachello-Dolmen, P.G., Soibelzon, E., Soibelzon, L., Todd, J.A., Vermeij, G.J., Jackson, J.B.C., 2016. Formation of the isthmus of Panama. Sci. Adv. 2 (8), e1600883 https://doi.org/10.1126/sciadv.1600883.

Ortiz-Jerónimo, C.G., Gómez-Espinosa, M.C., Gío-Argáez, F.R., Talavera-Mendoza, O., Flores de Dios, L.A., Martínez-Villa, B.B., 2021. Drilling predation on juvenile and adult gastropod shells during the Pliocene in the eastern Pacific, southern Mexico. J. South Am. Earth Sci. 110, 103352 https://doi.org/10.1016/j.jsames.2021.103352.

Pederson, C., Mavromatis, V., Dietzel, M., Rollion-Bard, C., Nehrke, G., Jons, N., Johum, K.P., Immenhauser, A., 2019. Diagenesis of mollusc aragonite and the role of fluid reservoirs. Earth Planet Sci. Lett. 514, 130–142. https://doi.org/10.1016/j.epsi.2019.02.038.

Peeters, F.J.C., Brummer, G.-J.A., Ganssen, G., 2002. The effect of upwelling on the distribution and stable isotope composition of Globigerina bulloides and Globigerinoides ruber (planktic foraminifera) in modern surface waters of the NW Arabian Sea. Global Planet. Change 34 (3–4), 269–291. https://doi.org/10.1016/s0921-8181(02)00120-0.

Pezelj, Đ., Sremac, J., Sokač, A., 2007. Palaeoecology of the late badenian foraminifera and ostracoda from the SW central paratethys (medvednica Mt., Croatia). Geologia Crotica 60 (2), 139–150. https://doi.org/10.4154/GC.2007.03.

Ponder, W.F., Lindberg, D.R., Ponder, J.M., 2019. Shell, body, and muscles. In: Ponder, W.F., Lindberg, D.R., Ponder, J.M. (Eds.), Biology and Evolution of the Mollusca. CRC Press, Boca Raton. https://doi.org/10.1201/9781351115667-3.

Prazeres, M., Roberts, T.E., Pandolfi, J.M., 2017. Variation in sensitivity of large benthic Foraminifera to the combined effects of ocean warming and local impacts. Sci. Rep. 7, 45227 https://doi.org/10.1038/srep45227.

Puckett, T.M., 2008. Ostracoda as indicators of vertebrate environments in the middle Eocene guys hill Formation of Jamaica. Micropaleontology 54 (2), 139–158. https://doi.org/10.47894/mpal.54.2.03.

Puotinen, M., Drost, E., Lowe, R., Depczynski, M., Radford, B., Heyward, A., Gilmour, J., 2020. Towards modelling the future risk of cyclone wave damage to the world's coral reefs. Global Change Biol. 26 (8), 4302–4315. https://doi.org/10.1111/gcb.15136.

Rahiminejad, A.H., Yazdi, M., Bahrami, A., 2020. Palaeoenvironments and taphonomy of clypeasteroids in Miocene carbonates of the esfahan–sirjan basin, central Iran. Facies 66. https://doi.org/10.1007/s10347-020-00598-6, 14.

Ramalho, L.V., Távora, V.A., Tilbrook, K.J., Zágoršek, K., 2015. New species of hippopleurifera (bryozoa, cheilostomata) from the Miocene Pirabas Formation, Pará state, Brazil. Zootaxa 3999 (1), 125–134. https://doi.org/10.11646/zootaxa.3999.1.8.

Ramalho, L.V., Távora, V.A., Zágoršek, K., 2017. New records of the bryozoan metrarabdotos from the Pirabas Formation (lower Miocene), Pará state, Brazil. Palaeontol. Electron. 1–11, 20.2.32A.

Ramalho, L.V., Serrano, F., Rueda, J.L., Távora, V.A., Zágoršek, K., 2019. New update on the bryozoan assemblage of the Miocene Pirabas Formation, Brazil. In: Schmidt, R., Reid, C.M., Gordon, D.P., Walker-Smith, G., Percival, I.P. (Eds.), Bryozoan Studies. Australasian Palaeontologists, Sydney, pp. 109–114.

Rossetti, D.F., 2001. Late Cenozoic sedimentary evolution in northeastern Pará, Brazil, within the context of sea level changes. J. South Am. Earth Sci. 14 (1), 77–89. https://doi.org/10.1016/S0895-9811(01)00008-6.

Rossetti, D.F., 2006. Evolução sedimentar miocênica nos estados do Pará e Maranhão. Geol. USP Série Científica, São Paulo 6 (2), 7–18. https://doi.org/10.5327/S1519-874X2006000300003.

Rossetti, D.F., Truckenbrodt, W., Góes, A.M., 1989. Estudo paleoambiental e estratigráfico dos sedimentos Barreiras e Pós-Barreiras na região Bragantina, nordeste do Pará. Bol. Mus. Para. Emílio Goeldi, Sér. Ciênc. Ter. 1 (1), 25–74.

Rossetti, D.F., Bezerra, F.H.R., Dominguez, J.M.L., 2013. Late Oligocene–Miocene transgressions along the equatorial and eastern margins of Brazil. Earth Sci. Rev. 123, 87–112. https://doi.org/10.1016/j.earscirev.2013.04.005.

Şafak, Ü., 2019. Paleoenvironmental features and ostracod investigation of Paleogene-Neogene sequences in Babaeski-Lüleburgaz-Muratlı-Çorlu region (Southeastern Thrace, Turkey). Bull. Miner. Res. Explor. 160, 45–79. https://doi.org/10.19111/bulletinofmre.502805.

Sariaslan, N., Langer, M.R., 2021. Atypical, high-diversity assemblages of foraminifera in a mangrove estuary in northern Brazil. Biogeosciences 18, 4073–4090. https://doi.org/10.5194/bg-18-4073-2021, 2021.

Stewart, J.A., James, R.H., Anand, P., Wilson, P.A., 2017. Silicate weathering and carbon cycle controls on the oligocene-miocene transition glaciation. Paleoceanography 32 (10), 1070–1085. https://doi.org/10.1002/2017PA003115.

Utida, G., Cruz, F.W., Etourneau, J., Bouloubassi, I., Schefuß, E., Vuille, M., Novello, V.F., Prado, L.F., Sifeddine, A., Klein, V., Zular, A., Viana, J.C.C., Turcq, B., 2019. Tropical South Atlantic influence on Northeastern Brazil precipitation and ITCZ displacement during the past 2300 years. Sci. Rep. 9 https://doi.org/10.1038/s41598-018-38003-6, 1698.

Vale, N.F., Braga, J.C., de Moura, R.L., Salgado, L.T., de Moraes, F.C., Karez, C.S., de Carvalho, R.T., Salomon, P.S., Menandro, P.S., Amado-Filho, G.M., Bastos, A.C., 2022. Distribution, morphology and composition of mesophotic 'reefs' on the Amazon Continental Margin. Mar. Geol. 447, 106779 https://doi.org/10.1016/j.margeo.2022.106779.

Vital, H., Stattegger, K., Amaro, V.E., Schwarzer, K., Frazão, E.P., Tabosa, W.F., Silveira, I.M., 2008. A modern high-energy siliciclastic-carbonate platform: continental shelf adjacent to northern Rio Grande do norte state, northeastern Brazil. In: Hampson, G.J., Steel, R.J., Burgess, P.M., Dalrymple, R.W. (Eds.), Recent Advances in Models of Siliciclastic Shallow-Marine Stratigraphy, vol. 90, pp. 175–188. https://doi.org/10.2110/pec.08.90.0177. Journal of Sedimentary Research.

Whatley, R.C., Watson, K., 1988. A preliminary account of the distribution of ostracoda in recent reef and reef associated environments in the pulau seribu or thousand island group, java sea. Dev. Palaeontol. Stratigr. 11, 399–411. https://doi.org/10.1016/S0920-5446(08)70197-3.

Wong, T.E., van Geuns, L., 2019. The discovery of a major hydrocarbon occurrence in the Guiana Basin, offshore Suriname: a blessing or a curse? Acad. J. Suriname 11 (1), 1–6. http://adekusjournal.com/ojs/index.php/acjoursu/article/view/6.

Yan, Q., Korty, R., Zhang, Z., Wang, H., 2019. Evolution of tropical cyclone genesis regions during the Cenozoic era. Nat. Commun. 10 https://doi.org/10.1038/s41467-019-11110-2, 3076.

Zachos, J., Pagan, M., Sloan, L., Thomas, E., Billups, K., 2001. Trends, rhythms, and aberrations in global climate 65 Ma to present. Science 292 (5517), 686–693. https://doi.org/10.1126/science.1059412.

Zágoršek, K., Ramalho, L.V., Berning, B., Távora, V.A., 2014. A new genus of the family Jaculinidae (Cheilostomata, Bryozoa) from the Miocene of the tropical western Atlantic. Zootaxa 3838 (1), 98–112. https://doi.org/10.11646/zootaxa.3838.1.5.

Zalán, P.V., Hodgson, N., Saunders, M., 2019. Foz do Amazonas and Pará-Maranhão basins ready to replicate Guyana success. 2019 AAPG Annual Convention and Exhibition, San Antonio, Texas. Search and Discovery 2019, 19–22. doi:10.1306/30624Zalan2019.